*American Mineralogist, Volume 94, pages 121–134, 2009*

# Multi-analytical approach to solve the puzzle of an allanite-subgroup mineral from Kesebol, Västra Götaland, Sweden

**Paola Bonazzi,[1,*] Dan Holtstam,[2,†] Luca Bindi,[3] Per Nysten,[4] and GianCarlo Capitani[5]**

[1]Dipartimento di Scienze della Terra, Università di Firenze, via La Pira 4, I-50121 Firenze, Italy
[2]Naturhistoriska riksmuseet, Box 50007, SE-104 05 Stockholm, Sweden
[3]Museo di Storia Naturale, Sezione di Mineralogia, Università di Firenze, via La Pira 4, I-50121 Firenze, Italy
[4]Department of Earth Sciences, Uppsala University, SE-752 36, Uppsala, Sweden
[5]Dipartimento Geomineralogico, Università di Bari, Via E. Orabona 4, I-70125, Bari, Italy

## Abstract

Dark-brownish, euhedral crystals of an "allanite-like" mineral occur in a hematite-impregnated Mn-silicate rock at Kesebol, Västra Götaland, Sweden, associated with gasparite-(Ce), chernovite-(Y), rhodonite, andradite, manganoan calcite, and quartz. A structural study was carried out on single crystals—untreated, heated in air, and heated under inert atmosphere—combined with Mössbauer spectroscopy and TEM investigation. In all the untreated crystals the mean <M3-O> distance indicates that $Me^{2+}$(Me = Mn, Fe) prevails at this site (<M3-O> in the range 2.169–2.180 Å), in contrast with chemical data obtained by EPMA that yield a simplified formula $Ca(REE^{3+}_{2/3}\square_{1/3})Me^{3+}_3(SiO_4)(Si_2O_7)O(OH)$, when normalized to Si = 3.00 apfu. Moreover, when a crystal is heated in air, all geometrical and structural variations indicate the development of an oxidation-dehydrogenation reaction, thus confirming that M3 is occupied by divalent cations before heating. The corresponding dehydrogenation is confirmed by a dramatic lengthening of the donor-acceptor distance. A crystal was annealed under inert atmosphere to verify possible effects of radiation damage on the polyhedral volumes. After prolonged annealing at 700 °C, a slight decrease of the unit-cell parameters is observed, suggesting restoring of crystallinity from a "partially metamict" state. Nonetheless, even in the annealed crystal, the <M3-O> distance is still consistent with a dominance of divalent cations at the M3 site. For all the examined crystals, structural data point to an octahedral cation population as follows: M1 = ($Me^{3+}$, Al); M2 = (Al, $Me^{3+}$); M3 = ($Me^{2+}$, $Me^{3+}$). This assumption is also in agreement with the Mössbauer spectrum, which was fitted to two Lorentzian quadrupole doublets for $Fe^{3+}$ and one for $Fe^{2+}$. Values of the isomer shifts (0.36 and 0.37 mm/s for $Fe^{3+}$; 1.11 mm/s for $Fe^{2+}$) and the quadrupole splitting (1.96 and 1.02 for $Fe^{3+}$; 1.90 for $Fe^{2+}$) show that $Fe^{2+}$ (~12% of the total iron) is located in M3, while $Fe^{3+}$ occupies M1 and, to lesser extent, M2. TEM-EDS investigations have revealed chemical heterogeneities related to different degree of radiation damage. In particular, areas showing poor crystallinity are relatively enriched in Si and O with respect to the highly crystalline areas, thus suggesting that EPMA chemical data are biased by the presence of metamict areas enriched in $SiO_2$ and likely in $H_2O$. EPMA data were therefore corrected for the excess of silica. The cation population after correction is in keeping with the structural and spectroscopic data. Disregarding minor substitutions, the ideal chemical formula for the epidote-group mineral from Kesebol is $CaREEFe^{3+}AlMn^{2+}(Si_2O_7)(SiO_4)O(OH)$, which is related to ferriallanite-(Ce) by the substitutional vector $^{M3}(Mn^{2+}) \rightarrow {}^{M3}(Fe^{2+})$.

**Keywords:** Epidote-group, allanite-subgroup, single-crystal X-ray diffraction, Mössbauer spectroscopy, transmission electron microscopy, metamictization

## Introduction

Allanite, ideally $^{A1}(Ca)^{A2}(REE)^{M1,M2}(Al)_2{}^{M3}(Fe^{2+})(SiO_4)(Si_2O_7)O(OH)$, is by far the most common REE-bearing member of the epidote-group minerals; in the last 20 years, however, several new REE-bearing members of the epidote group have been described. According to the recent IMA-approved revision of nomenclature of this group of minerals (Armbruster et al. 2006), any member that can be derived from clinozoisite, ideally $^{A1,A2}(Ca)_2{}^{M1,M2,M3}(Al)_3(SiO_4)(Si_2O_7)O(OH)$, by homovalent substitutions and one coupled heterovalent substitution of the type $^{A2}(REE^{3+}) + {}^{M3}(Me^{2+}) \rightarrow {}^{A2}(Ca^{2+}) + {}^{M3}(Me^{3+})$ has to be classified in the allanite sub-group. With Ca dominant in A1 and $Al^{3+}$ dominant in M1 and M2, the root names allanite (Thomson 1810) and dissakisite (Grew et al. 1991) refer to $Me^{2+} = Fe^{2+}$ and Mg, respectively. When other cations than Al dominate the M1 site, a proper prefix is added to the root name. Thus, ferriallanite (Kartashov et al. 2002) is the analog of allanite with $Fe^{3+}$ dominant in the octahedral M1 site. Despite the existence of a potential new member of the allanite sub-group with end-member formula $Ca(REE)AlAlMn^{2+}(SiO_4)(Si_2O_7)O(OH)$ (e.g., Cenki-Tok

* E-mail: paola.bonazzi@unifi.it
† Present address: Vetenskapsrådet, 103 78 Stockholm, Sweden.

et al. 2006; Table 1, analysis 5), to date no new root name has been officially assigned to the $Mn^{2+}$ analog of allanite, which occurs likely as local $Mn^{2+}$ enrichment in zoned allanite. Indeed, chemical formulae derived from analytical data of most of the manganoan allanite quoted in the literature (Deer et al. 1986) suggest that $Mn^{2+}$ is primarily replacing for Ca at the A1 site and $Fe^{2+}$ is still the dominant charge-balancing cation at M3. In other words, they are solid solutions between allanite and the new member recently approved by IMA with the name uedaite-(Ce) (Miyawaki et al. 2008), which has $Mn^{2+}$ dominant at the A1 site and $Fe^{2+}$ on M3. On the other hand, in extremely Mn-rich members from Mn-rich assemblages, $Mn^{2+}$ dominates both the M3 and the A1 sites. This is the case of manganiandrosite-(La) (Bonazzi et al. 1996) and manganiandrosite-(Ce) (Cenki-Tok et al. 2006), where M1 is occupied by dominant $Mn^{3+}$, and vanadoandrosite-(Ce) (Cenki-Tok et al. 2006), having M1 occupied by dominant $V^{3+}$.

In his article entitled "The mess that is allanite," Ercit (2002) pointed out the difficulties and errors in using the term "allanite" and assigning a proper name to REE-bearing epidote-group minerals. He also critically reviewed several methods reported in literature describing how to derive the formula from electron-microprobe analytical data. His evaluation resulted in a recommended procedure on the basis of $\Sigma(M + T)_{cations} = 6$. Nonetheless, this method fails for Mn-rich members, where $Mn^{2+}$ may be present in both the M3 octahedral site and in the large A1 site, which is a feature more common than expected by Ercit himself. For this reason, Armbruster et al. (2006) recommended normalization of electron-microprobe analytical data on the basis of $\Sigma(A + M + T)_{cations} = 8$. This method, however, is inadequate whenever A-site vacancies are present, which might be the case for partly or completely metamict material. Metamict samples, indeed, tend to be more susceptible to alteration than well-crystallized minerals (Gieré and Sorensen 2004) and may deviate significantly in composition and stoichiometry from their non-metamict counterparts. On the basis of chemical data, Peterson and MacFarlane (1993) estimated varying degrees of vacancy at the A sites (up to 0.439 apfu) of most metamict allanite specimens ($ThO_2$ up to 4.16 wt%) from granitic rocks and calcite veins in the Grenville Province of the Canadian Shield. Because the transition from an ideal crystal to amorphous material during metamictization is continuous, the chemical changes—hydration, swelling, and selective leaching—usually accompanying the loss of crystallinity and possibly leading to vacancies can be unsuspected when the samples are still optically rather fresh and diffraction quality is still good. Interestingly, significant A-site vacancies were also calculated from electron-microprobe analytical data (Chesner and Ettlinger 1989) on young, optically rather fresh, volcanic allanite ($ThO_2$ up to 2.17 wt%). A-site vacancies were also hypothesized in allanite-(Ce) from different granitic rocks in Japan showing different degrees of radiation damage (Hoshino et al. 2006). However, since in that case the chemical formulae were calculated on the basis of $\Sigma(M + T)_{cations} = 6$ in spite of the presence of high contents of $Mn^{2+}$ likely substituting for Ca, the actual presence of vacancies is difficult to ascertain. Provided the low occupancy of the A sites is not an artifact of formula calculation, and no element is missing in the analysis, the presence of A-site vacancies could indeed represent an additional mechanism to charge-balance the incorporation of $REE^{3+}$ in the structure of the epidote-group minerals. Depending on whether vacancies are ordered on A1 (*i*) or A2 (*ii*), the following substitution vectors could be taken into consideration: $^{A1}(Ca) + {}^{A2}(Ca) \leftrightarrow {}^{A1}(Ca_{1/2}\square_{1/2}) + {}^{A2}(REE^{3+})$ (*i*) or $^{A2}(Ca) \leftrightarrow {}^{A2}(REE^{3+}_{2/3} + \square_{1/3})$ (*ii*). These mechanisms relate the clinozoisite sub-group members to a set of hypothetical end-members as follows: $(Ca_{1/2}\square_{1/2})REE^{3+}M^{3+}_3(SiO_4)(Si_2O_7)O(OH)$ (*i*) or $Ca(REE^{3+}_{2/3}\square_{1/3})M^{3+}_3(SiO_4)(Si_2O_7)O(OH)$ (*ii*). Note that both of these components, unlike the allanite sub-group minerals, are devoid of $Me^{2+}$ at the octahedral sites. According to Ercit (2002), appreciable proportions of the $(Ca_{1/2}\square_{1/2})REE^{3+}M^{3+}_3(SiO_4)(Si_2O_7)O(OH)$ component could be inferred from chemical data quoted in the literature of several REE-bearing members of epidote group, when properly normalized. Moreover, only in few cases A-site vacancies were supported by the results of structure refinements from single-crystal X-ray diffraction (Sokolova et al. 1991; Hoshino et al. 2005); even in these cases, however, due to the complexity of cation sub-

**TABLE 1.** Average electron microprobe analyses (with standard deviations in parentheses) of selected fragments of the epidote-group mineral from Kesebol

| | K1*‡ | K2*‡ | K1*§ | K2*§ | k3†§ | k4†§ | k5†§ |
|---|---|---|---|---|---|---|---|
| *n* | 3 | 5 | 3 | 4 | 8 | 8 | 8 |
| $SiO_2$ | 31.72(1.46) | 31.32(0.62) | 30.55(1.38) | 30.57(0.72) | 30.98(0.58) | 31.15(0.54) | 30.76(0.60) |
| $TiO_2$ | n.a. | n.a. | 0.48(0.20) | 0.52(0.19) | 0.68(0.09) | 0.77(0.10) | 0.62(0.09) |
| $Al_2O_3$ | 9.53(0.44) | 9.13(0.31) | 8.62(0.47) | 8.63(0.28) | 8.97(0.26) | 9.03(0.45) | 8.90(0.38) |
| MgO | 0.49(0.11) | 0.45(0.05) | 0.46(0.12) | 0.45(0.04) | 0.35(0.09) | 0.36(0.07) | 0.40(0.07) |
| MnO | 9.44(0.27) | 9.31(0.16) | 9.44(0.25) | 9.22(0.14) | 9.56(0.13) | 9.57(0.18) | 9.22(0.11) |
| FeO | 11.99(0.59) | 12.85(0.16) | 13.44(0.57) | 13.44(0.21) | 13.91(0.40) | 13.95(0.41) | 13.70(0.33) |
| $La_2O_3$ | 1.71(0.14) | 1.23(0.12) | 0.99(0.15) | 0.89(0.10) | 0.87(0.09) | 0.91(0.08) | 1.06(0.10) |
| $Ce_2O_3$ | 15.45(1.55) | 14.64(0.43) | 15.52(1.24) | 14.39(0.58) | 13.69(0.37) | 14.02(0.50) | 14.95(0.55) |
| $Pr_2O_3$ | 0.60(0.02) | 0.70(0.09) | 1.18(0.03) | 1.62(0.04) | 1.14(0.12) | 0.71(0.06) | 0.95(0.01) |
| $Nd_2O_3$ | 3.48(0.11) | 5.55(0.34) | 4.76(0.12) | 4.81(0.41) | 4.04(0.40) | 4.30(0.35) | 4.70(0.44) |
| $Sm_2O_3$ | 0.38(0.03) | 0.77(0.04) | 0.74(0.04) | 0.50(0.03) | 0.56(0.05) | 0.67(0.04) | 0.74(0.05) |
| $Gd_2O_3$ | 0.13(0.01) | 0.17(0.06) | 0.02(0.01) | 0.16(0.06) | 0.12(0.05) | 0.06(0.02) | 0.20(0.08) |
| CaO | 8.79(0.36) | 8.59(0.15) | 8.88(0.41) | 8.60(0.20) | 9.35(0.25) | 9.36(0.25) | 9.22(0.29) |
| PbO | 0.62(0.20) | 0.22(0.10) | 0.38(0.12) | 0.23(0.09) | 0.26(0.11) | 0.27(0.13) | 0.28(0.13) |
| Total | 94.33(0.56) | 94.93(0.69) | 95.46(0.49) | 94.03(0.65) | 94.48(0.51) | 95.13(0.38) | 95.70(0.40) |

*Notes*: *n* = number of spots; n.a.= not analyzed.
* Single crystal used for structural study.
† Fragment from which the corresponding single crystal was selected.
‡ Cameca SX50 electron microprobe.
§ Jeol JXA-8600 electron microprobe.

stitutions in these minerals, other cation combinations involving full occupancy in the A sites may correspond to the same X-ray site-scattering powers. Up to date, no reliable structural proof of significant solid solution of the above component is reported. For these reasons, we were intrigued by a new recovery of an allanite-like mineral from Kesebol, Västra Götaland, Sweden (collected by Kjell Gatedal) for which chemical data pointed to an ideal formula $Ca(REE^{3+}_{2/3}\square_{1/3})M^{3+}_3(SiO_4)(Si_2O_7)O(OH)$ (Nysten and Holtstam 2005). To test this hypothesis, a structural study was carried out on single crystals—untreated, heated in air, and heated under inert atmosphere—combined with Mössbauer and infrared spectroscopy, and TEM investigation.

## Occurrence and geologic setting

The Kesebol deposit is one of a group of small Mn mineralizations found along the western shore of Lake Vänern in Västra Götaland County, west-central Sweden. Approximately 40 000 tons of manganese ore were produced at Kesebol during the mining period (1918–1944), along with lesser amounts of Cu (Geijer 1961). The ores are hosted within metavolcanic rhyolitic rocks of the Åmål Group, comprising ca. 1600 Ma old supracrustal units within the Southwest Scandinavian Domain of the Baltic Shield. During the Sveconorwegian orogeny, from 1200 to 900 Ma, tectonometamorphic and metallogenic processes took place in the region (Andréasson et al. 1987).

The Kesebol ores constitute epigenetic replacement and fracture-filling mineralization localized in a north-south shear zone. The Mn ores consist of two, essentially spatially separated components: oxide mineralization (hausmannite ± jacobsite) and carbonate-silicate mineralization (rhodochrosite + manganoan calcite + rhodonite + manganoan garnet). The oxide minerals are generally fine grained (≤0.1 mm). $Mn^{4+}$-bearing oxides and hydrous Mn silicates in veins have formed by alteration at a late stage. Cu ore is restricted to spatially limited sulfide-rich zones in the deposit.

The allanite-like mineral occurs as essentially euhedral crystals, exceptionally up to 5 mm long, in calcite-filled centimeter-sized vugs of a fractured Mn-silicate-hematite rock. Manganoan andradite, rhodonite, quartz, gasparite-(Ce), and minor chernovite-(Y) also belong to the mineral assemblage of these particular vugs. Gasparite-(Ce) from the sample investigated here (cat. no. 20020009) was previously chemically and structurally characterized by Kolitsch et al. (2004).

## Experimental methods

### Chemical analyses

The chemical composition of two crystals used for the structural study (K1 and K2, see below) were obtained by electron-microprobe analyses with a Cameca SX50 instrument operated at 20 kV and 20 nA (Department of Earth Sciences, Uppsala University). The time of measurement for element and background, respectively, was 20 s or longer. Standards used were pure synthetic REE phosphates ($L\alpha$ for La, Ce; $L\beta$ for other REE), vanadinite (Pb$M\beta$), $Fe_2O_3$ (Fe$K\alpha$), $MnTiO_3$ (Mn$K\alpha$), wollastonite (Ca$K\beta$), $Al_2O_3$ (Al$K\alpha$), MgO (Mg$K\alpha$), and albite (Si$K\alpha$). Raw data were processed in a Cameca version of the PAP (Pouchou and Pichoir 1991) routine. Strontium, Y, HREE, and Th were generally found to be below the detection limit.

Data were preliminarily recalculated following the site-assignment procedure recently approved by IMA (Armbruster et al. 2006), i.e., Σ of cations = 8 apfu and $Me^{2+}/Me^{3+}$ (Me = Mn, Fe) partitioned to balance 25 negative charges. With this method, however, a large excess of Si (>3.20 apfu) was found, indicating presence of A-site vacancies or incomplete element determination. The possible presence of light elements (Li, B, Be) was checked by laser ablation inductively coupled plasma—mass spectrometry (LA-ICP-MS) at the C.N.R.-Istituto di Geoscienze e Georisorse of Pavia. The instrument couples a 266 nm Nd:YAG laser source (Brilliant-Quantel) to a quadrupole ICP-MS (DRCe-PerkinElemer). $^6$Li, $^7$Li, $^9$Be, and $^{11}$B were acquired in peak hopping mode with a dwell time of 10 ms. Each analysis consisted in the acquisition of 30 s of background and 1 min of signal. Data reduction was carried out with the Glitter software (van Achterberg et al. 2001). Very low amounts of these elements (Li ≤ 5 ppm, Be ≤ 17.2 ppm, B ≤ 254 ppm) were found. Material paucity prevented direct determination of $H_2O$. Chemical data were repeated by means of a Jeol JXA-8600 electron microprobe (CNR-IGG, Firenze). The presence of minor elements was carefully checked. However, besides the elements already measured, only Ti was found and included in the working file (Table 1). For the other elements, the values were found to be fairly similar to those previously measured (Table 1). Besides K1 and K2 crystals, three grains (i.e., k3, k4, and k5) were embedded in resin and analyzed. Elements were determined at 15 kV accelerating voltage and 20 nA beam current, with 30 s as counting time. The analyses were performed on $K\alpha$ lines for light elements (Mg, Al, Si, Ca, Ti, Mn, Fe), $L\alpha$ for Y, and $M\alpha$ lines for Pb and Th. To avoid intra-REE interferences, La and Ce were determined on $L\alpha$ lines, while Pr, Nd, Sm, and Gd on $L\beta$ lines. The standards employed were olivine (Mg), albite (Al), kaersutite (Si, Ca, Fe), rutile (Ti), bustamite (Mn), and galena (Pb). The REE standards used were glasses of Drake and Weill (1972). Table 1 reports the chemical data obtained (average values). Derivation of the chemical formula will be discussed below, taking into account the results of structural data, Mössbauer spectroscopy, and TEM investigations.

### X-ray data collection and thermal annealing

Several fragments of the same mineral grain were tested for diffraction quality, among which K1 and K2 crystals were selected. Later, K3, K4, and K5 crystals were also selected from the k3, k4, and k5 grains removed from the resin. Unit-cell parameters were determined by means of least-squares refinement of the setting angles of 25 reflections ($16.3 < \theta < 29.5°$) measured with an Enraf Nonius CAD4 single-crystal diffractometer (Table 2). X-ray intensity data were obtained at room temperature from untreated crystals K1, K2, K4, and K5, crystal K3 heated in air, and crystal K5 heated under inert atmosphere, using graphite-monochromatized Mo$K\alpha$ radiation under the experimental conditions listed in Table 2. K3 crystal was annealed in air for 48 h at selected temperatures ranging from 400 to 900 °C using a magnetic release furnace that allows rapid cooling to room temperature. After each heat treatment, unit-cell parameters were determined (Table 2), whereas the whole intensity data collection was carried out only when significant variations of the unit cell occurred. After the annealing at 900 °C, reflections appeared broad and very weak, and the unit cell was not determined. K5 was annealed under inert atmosphere ($N_2$) for 20 h at 600 °C and for 20 h at 700 °C using a gas mixing vertical furnace. Diffraction intensity data were collected after both treatments. A further annealing at 700 °C for 10 h was performed under the same conditions but no significant variation of the unit-cell parameters was observed.

### Structure refinements

Intensity data were corrected for absorption following the semi-empirical method of North et al. (1968) and subsequently treated for Lorentz-polarization effects. Structure refinements were carried out in space group $P2_1/m$ using SHELXL-97 (Sheldrick 1997). Site-scattering values were refined using scattering curves (*International Tables for X-ray Crystallography*, Ibers and Hamilton 1974) for fully ionized species for A and M sites [$Ca^{2+}$ vs. $Mn^{2+}$(A1), $Ca^{2+}$ vs. $Ce^{3+}$(A2), $Al^{3+}$ vs. $Mn^{3+}$(M1), $Al^{3+}$ vs. $Fe^{3+}$(M2), and $Al^{3+}$ vs. $Mn^{2+}$(M3)]; following the choice adopted by Lavina et al. (2006) for the structural refinement of dissakisite-(La), partially ionized curves were used for tetrahedral ($Si^{2.5+}$) and anion ($O^{1-}$) sites. An isotropic model was adopted during the first least-squares cycles; after convergence was achieved using an anisotropic model, the difference- Fourier map was carefully examined to locate the hydrogen atom. Only in the case of the crystal annealed under inert atmosphere (K5-700*) was a peak having atomic coordinates close to those commonly found for the allanite structure (Bonazzi and Menchetti 1995) located on the difference-Fourier map and subsequently added in the model. Refined atomic parameters (H site) were $x = 0.018(5)$, $y = ¼$, $z = 0.293(4)$, $U_{eq} = 0.022(9)$. For all the untreated crystals and for the crystals heated at $T < 700$ °C, an additional "ghost" peak (0.8–1.3 e$^-$/Å$^3$) was observed at $x \sim 0.17(\pm0.01)$, $y = ¼$, $z \sim 0.31(\pm0.02)$ at ~2.0 Å from M3. For all data sets but K5-700* the parameters refined in the final cycles were scale factor, atomic coordinates, anisotropic displacement parameters, and occupancy of A and M sites; the adopted weighting

**TABLE 2.** Crystal data and experimental details

| | K1 | K2 | K4 | K5 | K5-600* | K5-700* | K3 | K3-400 |
|---|---|---|---|---|---|---|---|---|
| *a* (Å) | 8.971(2) | 8.943(3) | 8.958(3) | 8.953(1) | 8.950(2) | 8.925(3) | 8.949(3) | 8.932(8) |
| *b* (Å) | 5.766(2) | 5.768(1) | 5.764(2) | 5.763(1) | 5.770(1) | 5.744(1) | 5.758(1) | 5.735(2) |
| *c* (Å) | 10.224(2) | 10.195(4) | 10.205(2) | 10.186(4) | 10.194(3) | 10.158(2) | 10.204(6) | 10.223(8) |
| β (°) | 114.53(2) | 114.42(3) | 114.50(2) | 114.42(2) | 114.42(2) | 114.46(2) | 114.58(3) | 114.85(4) |
| $V_{cell}$ (Å$^3$) | 481.1(2) | 478.8(3) | 479.5(3) | 478.5(2) | 479.3(2) | 474.0(2) | 478.1(3) | 475.2(6) |
| size (μm) | 120 × 120 × 180 | 120 × 150 × 180 | 120 × 160 × 200 | 190 × 220 × 300 | 190 × 220 × 300 | 190 × 220 × 300 | 120 × 160 × 180 | 120 × 160 × 180 |
| $\theta_{max}$ (Mo*K*α) | 35 | 35 | 35 | 35 | 35 | 35 | | |
| $R_{int}$ (%) | 3.85 | 5.90 | 3.46 | 2.90 | 3.77 | 2.26 | | |
| $R_{obs}$ (%) | 3.67 | 4.90 | 3.80 | 3.22 | 3.20 | 2.10 | | |
| no. obs. refl. | 1777 | 1563 | 1803 | 1896 | 1865 | 1981 | | |
| $R_{all}$ (%) | 5.54 | 8.17 | 5.39 | 4.44 | 4.35 | 2.65 | | |
| no. indep. refl. | 2287 | 2271 | 2275 | 2278 | 2277 | 2270 | | |

| | K3-500 | K3-550 | K3-600 | K3-650 | K3-700 | K3-750 | K3-800 | K3-850 |
|---|---|---|---|---|---|---|---|---|
| *a* (Å) | 8.919(9) | 8.922(6) | 8.908(5) | 8.905(4) | 8.891(5) | 8.896(6) | 8.894(7) | 8.891(5) |
| *b* (Å) | 5.727(3) | 5.717(4) | 5.711(2) | 5.709(2) | 5.696(3) | 5.699(5) | 5.699(5) | 5.689(3) |
| *c* (Å) | 10.266(9) | 10.272(9) | 10.314(9) | 10.335(4) | 10.350(9) | 10.352(9) | 10.368(9) | 10.377(7) |
| β (°) | 115.03(5) | 115.24(6) | 115.38(4) | 115.37(3) | 115.35(4) | 115.69(7) | 115.69(8) | 115.65(3) |
| $V_{cell}$ (Å$^3$) | 475.1(7) | 473.9(7) | 474.1(5) | 474.7(2) | 473.7(6) | 473(1) | 474(1) | 473(1) |
| size (μm) | 120 × 160 × 180 | 120 × 160 × 180 | 120 × 160 × 180 | 120 × 160 × 180 | 120 × 160 × 180 | 120 × 160 × 180 | 120 × 160 × 180 | |
| $\theta_{max}$ (Mo*K*α) | | 35 | 32 | | 32 | | 32 | |
| $R_{int}$ (%) | | 2.44 | 5.83 | | 3.17 | | 4.48 | |
| $R_{obs}$ (%) | | 3.62 | 4.13 | | 2.38 | | 3.96 | |
| no. obs. refl. | | 2020 | 1340 | | 1633 | | 1627 | |
| $R_{all}$ (%) | | 4.07 | 6.67 | | 2.67 | | 4.29 | |
| no. indep. refl. | | 2277 | 1798 | | 1793 | | 1791 | |

*Note:* Unit-cell determination and intensity data collections were done at room temperature on untreated crystals and crystals heated ex situ.
* Denotes annealing under inert atmosphere.

scheme was $w = 1/[\sigma^2(F_o^2) + (k_1p)^2 + k_2p]$, where $p = \text{Max}(F_o^2 + 2F_c^2)/3$ and $k_1$ and $k_2$ are refined parameters. This made a total of 121 least squares variables (125 for K5-700*). Details of refinements are given in Table 2. Fractional coordinates and anisotropic displacement parameters are given in Tables 3 and 4, respectively, for both K5 and K5-700*. Table 5 lists the atomic coordinates and the anisotropic displacement parameters for the other refinements.[1]

### Mössbauer spectroscopy

A spectrometer system with a $^{57}$Co point (~8 mCi) source, a proportional counter and a multi-channel analyzer was used to obtain $^{57}$Fe transmission Mössbauer data for an untreated powder sample (2 mg). Two mirror-image spectra with a velocity span of ±4.3 mm/s were collected at room temperature over 1024 channels. A foil of metallic iron was used for velocity calibration and as isomer-shift reference. Spectra were reduced and fitted using updated versions of the MDR and MDA programs (Jernberg and Sundqvist 1983), assuming Lorentzian shapes and equal width and intensity of each quadrupole line pair. Site fraction calculations were done under the assumption of identical recoil-free fractions for all Fe atoms.

### Fourier-transform infrared microspectroscopy

A polarized FTIR spectrum was collected with a spectral resolution of 2 cm$^{-1}$ on a non-oriented single-crystal fragment thinned to 24 μm, with a Bruker Equinox55 microscope-spectrometer equipped with a KBr beamsplitter and a mercury-cadmium-telluride detector.

### Transmission electron microscopy

TEM mounts were prepared from mineral fragments mechanically thinned to a thickness of 20–30 μm. Electron transparency was achieved by argon ion-milling at low angle with a Gatan PIPS. Finally, to avoid electrostatic charging in the TEM, the samples were carbon coated. TEM investigations were performed with a JEOL-JEM 2010 at the Dipartimento Geomineralogico of the University of Bari (point resolution ~2.0 Å). Images were recorded with a Gatan MSC794 CCD camera. TEM compositional spectra were obtained with an Oxford LINK energy dispersive X-ray spectrometer (EDS).

The elements O, Mg, Al, Si, Ca, Mn, Fe, Ce, and Nd were quantified by using theoretical *k*-factors in the INCA spectrum analyzer software. Care was taken to make results internally consistent. The electron dose was maintained as far as possible constant from place to place by always using the same spot size, acquisition time, and mean counting rate. To avoid any differential absorption among different analyzed areas, chemical raw concentrations were corrected for thickness effects using the "electron neutrality criterion" (Van Cappellen and Doukhan 1994). Basically, through a trial-and-error routine, we searched for the unique thickness for which the weighted sum of anion and cation valences cancels out because of the different elemental mass-absorption coefficients.

## RESULTS

### Chemical composition: Tentative chemical formula

Normalization to Σ of cations = 8 apfu of the chemical data reported in Table 1, even in the case of more complete analyses (see footnote §), leads to a considerable excess of Si (3.09–3.12 apfu). Assuming homogeneity of the mineral phase, excess of Si might indicate either incomplete element determination or presence of A-site vacancies, or both. As the presence of elements unusually reported for epidote-group minerals, including light elements, was carefully checked, the presence of vacancies at the A sites was taken into consideration. In such a case, the empirical formula could be better calculated on the basis of a fixed number of tetrahedral + octahedral cations (the superior method no. 10 of Ercit 2002). Nonetheless, the presence of high amounts of Mn (MnO ranging from 9.22 to 9.57 wt%), and the fact that Mn may be present as $Mn^{2+}$ and $Mn^{3+}$ in the octahedral sites and as $Mn^{2+}$ in the large A1 site hampers the use of this method. Following the method recommended for cases with Si > 3.05 apfu (Armbruster et al. 2006), the formula was renormalized on

[1] Deposit item AM-09-004, Table 5 (atomic coordinates and the anisotropic displacement parameters). Deposit items are available two ways: For a paper copy contact the Business Office of the Mineralogical Society of America (see inside front cover of recent issue) for price information. For an electronic copy visit the MSA web site at http://www.minsocam.org, go to the American Mineralogist Contents, find the table of contents for the specific volume/issue wanted, and then click on the deposit link there.

**TABLE 3.** Site occupancies, fractional atomic coordinates, and equivalent isotropic displacement parameters (Å$^2$) for K5 and K5-700*

| | K5 | | | | | K5-700* | | | | |
|---|---|---|---|---|---|---|---|---|---|---|
| Atom | Occupancy | *x* | *y* | *z* | $U_{iso}$ | Occupancy | *x* | *y* | *z* | $U_{iso}$ |
| A1 | 0.52Mn + 0.48Ca | 0.7602(1) | 0.75000 | 0.15245(9) | 0.0192(2) | 0.52Mn + 0.48Ca | 0.76071(6) | 0.75000 | 0.15180(5) | 0.0116(1) |
| A2 | 0.78Ce + 0.22Ca | 0.59396(4) | 0.75000 | 0.42667(3) | 0.01797(9) | 0.78Ce + 0.22Ca | 0.59496(2) | 0.75000 | 0.42657(2) | 0.01164(5) |
| M1 | 0.78Mn + 0.22Al | 0.00000 | 0.00000 | 0.00000 | 0.0142(2) | 0.78Mn + 0.22Al | 0.00000 | 0.00000 | 0.00000 | 0.0088(1) |
| M2 | 0.86Al + 0.14Fe | 0.00000 | 0.00000 | 0.50000 | 0.0130(3) | 0.86Al + 0.14Fe | 0.00000 | 0.00000 | 0.50000 | 0.0083(2) |
| M3 | 1.00Mn | 0.30948(9) | 0.25000 | 0.21307(8) | 0.0179(2) | 1.00Mn | 0.30626(5) | 0.25000 | 0.21377(4) | 0.00972(9) |
| Si1 | | 0.3443(1) | 0.75000 | 0.0374(1) | 0.0128(2) | | 0.34464(8) | 0.75000 | 0.03876(7) | 0.0079(1) |
| Si2 | | 0.6914(1) | 0.25000 | 0.2793(1) | 0.0133(2) | | 0.68996(8) | 0.25000 | 0.27864(7) | 0.0078(1) |
| Si3 | | 0.1908(1) | 0.75000 | 0.3254(1) | 0.0117(2) | | 0.19090(8) | 0.75000 | 0.32504(7) | 0.0067(1) |
| O1 | | 0.2402(3) | 0.9894(4) | 0.0273(3) | 0.0198(5) | | 0.2409(2) | 0.9898(2) | 0.0292(2) | 0.0129(3) |
| O2 | | 0.3147(3) | 0.9729(4) | 0.3635(2) | 0.0181(4) | | 0.3148(2) | 0.9733(2) | 0.3634(1) | 0.0110(2) |
| O3 | | 0.8017(3) | 0.0150(4) | 0.3332(3) | 0.0200(5) | | 0.8004(2) | 0.0149(2) | 0.3334(2) | 0.0128(2) |
| O4 | | 0.0578(4) | 0.25000 | 0.1353(4) | 0.0175(6) | | 0.0562(2) | 0.25000 | 0.1339(2) | 0.0108(3) |
| O5 | | 0.0494(4) | 0.75000 | 0.1565(3) | 0.0170(6) | | 0.0497(2) | 0.75000 | 0.1561(2) | 0.0102(3) |
| O6 | | 0.0760(4) | 0.75000 | 0.4169(4) | 0.0156(6) | | 0.0757(2) | 0.75000 | 0.4166(2) | 0.0106(3) |
| O7 | | 0.5131(4) | 0.75000 | 0.1781(4) | 0.0201(6) | | 0.5143(2) | 0.75000 | 0.1786(2) | 0.0134(4) |
| O8 | | 0.5504(5) | 0.25000 | 0.3376(5) | 0.0316(9) | | 0.5486(3) | 0.25000 | 0.3359(2) | 0.0220(5) |
| O9 | | 0.6093(4) | 0.25000 | 0.1027(4) | 0.0241(7) | | 0.6098(3) | 0.25000 | 0.1016(2) | 0.0174(4) |
| O10 | | 0.0911(4) | 0.25000 | 0.4331(4) | 0.0158(6) | | 0.0913(2) | 0.25000 | 0.4329(2) | 0.0103(3) |
| H | | – | – | – | – | | 0.018(5) | 0.25000 | 0.293(4) | 0.02(1) |

* Denotes annealing ex situ under inert atmosphere.

**TABLE 4.** Anisotropic displacement parameters $U_{ij}$ (Å$^2$) for K5 and K5-700*

| Atom | $U_{11}$ | $U_{22}$ | $U_{33}$ | $U_{23}$ | $U_{13}$ | $U_{12}$ |
|---|---|---|---|---|---|---|
| | | | **K5** | | | |
| A1 | 0.0280(4) | 0.0130(3) | 0.0210(4) | 0.0000 | 0.0147(3) | 0.0000 |
| A2 | 0.0141(1) | 0.0212(2) | 0.0162(1) | 0.0000 | 0.00381(9) | 0.0000 |
| M1 | 0.0119(3) | 0.0116(3) | 0.0174(3) | –0.0007(2) | 0.0046(2) | –0.0012(2) |
| M2 | 0.0109(5) | 0.0099(5) | 0.0169(5) | –0.0006(4) | 0.0045(4) | –0.0003(4) |
| M3 | 0.0149(3) | 0.0144(3) | 0.0173(3) | 0.0000 | –0.0003(3) | 0.0000 |
| Si1 | 0.0124(5) | 0.0101(5) | 0.0138(5) | 0.0000 | 0.0032(4) | 0.0000 |
| Si2 | 0.0127(5) | 0.0107(5) | 0.0158(5) | 0.0000 | 0.0052(4) | 0.0000 |
| Si3 | 0.0106(4) | 0.0108(5) | 0.0137(5) | 0.0000 | 0.0051(4) | 0.0000 |
| O1 | 0.0184(9) | 0.0126(9) | 0.028(1) | 0.0018(9) | 0.0095(9) | 0.0021(8) |
| O2 | 0.0168(9) | 0.018(1) | 0.019(1) | –0.0005(8) | 0.0063(8) | –0.0034(8) |
| O3 | 0.0182(9) | 0.0112(9) | 0.023(1) | –0.0018(8) | 0.0009(8) | 0.0005(8) |
| O4 | 0.017(1) | 0.013(1) | 0.019(1) | 0.0000 | 0.004(1) | 0.0000 |
| O5 | 0.017(1) | 0.016(1) | 0.016(1) | 0.0000 | 0.004(1) | 0.0000 |
| O6 | 0.015(1) | 0.014(1) | 0.021(1) | 0.0000 | 0.011(1) | 0.0000 |
| O7 | 0.019(1) | 0.020(1) | 0.015(1) | 0.0000 | 0.001(1) | 0.0000 |
| O8 | 0.021(2) | 0.050(3) | 0.030(2) | 0.0000 | 0.017(2) | 0.0000 |
| O9 | 0.023(2) | 0.030(2) | 0.019(2) | 0.0000 | 0.009(1) | 0.0000 |
| O10 | 0.013(1) | 0.015(1) | 0.020(1) | 0.0000 | 0.008(1) | 0.0000 |
| | | | **K5-700*** | | | |
| A1 | 0.0177(2) | 0.0094(2) | 0.0107(2) | 0.0000 | 0.0088(2) | 0.0000 |
| A2 | 0.00907(7) | 0.01519(8) | 0.00884(7) | 0.0000 | 0.00190(5) | 0.0000 |
| M1 | 0.0073(2) | 0.0084(2) | 0.0094(2) | –0.0006(1) | 0.0023(1) | –0.0006(1) |
| M2 | 0.0069(3) | 0.0070(3) | 0.0094(3) | –0.0004(2) | 0.0019(2) | 0.0001(1) |
| M3 | 0.0073(2) | 0.0095(2) | 0.0084(2) | 0.0000 | –0.0007(1) | 0.0000 |
| Si1 | 0.0075(3) | 0.0069(3) | 0.0079(3) | 0.0000 | 0.0019(2) | 0.0000 |
| Si2 | 0.0065(3) | 0.0082(3) | 0.0085(3) | 0.0000 | 0.0028(2) | 0.0000 |
| Si3 | 0.0054(3) | 0.0074(3) | 0.0070(3) | 0.0000 | 0.0024(2) | 0.0000 |
| O1 | 0.0113(5) | 0.0089(6) | 0.0186(6) | 0.0009(5) | 0.0064(5) | 0.0022(5) |
| O2 | 0.0098(5) | 0.0114(6) | 0.0114(5) | –0.0010(4) | 0.0039(4) | –0.0026(4) |
| O3 | 0.0103(5) | 0.0076(6) | 0.0150(6) | –0.0013(5) | –0.0002(4) | 0.0003(4) |
| O4 | 0.0099(7) | 0.0103(8) | 0.0107(8) | 0.0000 | 0.0027(6) | 0.0000 |
| O5 | 0.0090(7) | 0.0105(8) | 0.0091(7) | 0.0000 | 0.0018(6) | 0.0000 |
| O6 | 0.0109(8) | 0.0104(8) | 0.0134(8) | 0.0000 | 0.0078(7) | 0.0000 |
| O7 | 0.0110(8) | 0.0160(9) | 0.0087(7) | 0.0000 | –0.0004(6) | 0.0000 |
| O8 | 0.0134(9) | 0.038(1) | 0.020(1) | 0.0000 | 0.0117(8) | 0.0000 |
| O9 | 0.0174(9) | 0.027(3) | 0.0093(8) | 0.0000 | 0.0064(7) | 0.0000 |
| O10 | 0.0088(7) | 0.0102(8) | 0.0126(8) | 0.0000 | 0.0051(6) | 0.0000 |

* Denotes annealing ex situ under inert atmosphere.

**TABLE 6.** Tentative chemical formulae for the epidote-group mineral from Kesebol

| | K1* | K2* | k3† | k4† | k5† |
|---|---|---|---|---|---|
| Si | 3.00 | 3.00 | 3.00 | 3.00 | 3.00 |
| $Ti^{4+}$ | 0.04 | 0.04 | 0.05 | 0.06 | 0.05 |
| Al | 1.00 | 1.00 | 1.02 | 1.03 | 1.02 |
| $Mn^{3+}$ | 0.42 | 0.61 | 0.57 | 0.53 | 0.43 |
| $Fe^{3+}$ | 1.10 | 1.10 | 1.13 | 1.12 | 1.12 |
| Mg | 0.07 | 0.07 | 0.05 | 0.05 | 0.06 |
| $Mn^{2+}$ | 0.37 | 0.16 | 0.21 | 0.25 | 0.33 |
| ΣM | 3.00 | 2.98 | 3.03 | 3.04 | 3.01 |
| $\Sigma e^-$(M) | 63.1 | 62.6 | 63.8 | 63.9 | 63.2 |
| La | 0.04 | 0.03 | 0.03 | 0.03 | 0.04 |
| $Ce^{3+}$ | 0.56 | 0.52 | 0.49 | 0.49 | 0.53 |
| Pr | 0.04 | 0.06 | 0.04 | 0.03 | 0.03 |
| Nd | 0.17 | 0.17 | 0.14 | 0.15 | 0.16 |
| Sm | 0.03 | 0.02 | 0.02 | 0.02 | 0.02 |
| Gd | 0.00 | 0.01 | 0.00 | 0.00 | 0.01 |
| ΣREE | 0.84 | 0.81 | 0.72 | 0.72 | 0.79 |
| Ca | 0.93 | 0.90 | 0.97 | 0.97 | 0.96 |
| $Pb^{2+}$ | 0.01 | 0.01 | 0.01 | 0.01 | 0.01 |
| ΣA | 1.78 | 1.72 | 1.70 | 1.70 | 1.76 |
| $\Sigma e^-$(A) | 68.6 | 66.3 | 62.4 | 62.4 | 66.3 |

*Notes:* Atomic ratios calculated from data reported in Table 1 on the basis of Si = 3.00; $Mn^{2+}$-$Mn^{3+}$ partition to balance 25 negative charges. $\Sigma e^-$(M) and $\Sigma e^-$(A) refer to sum of electron number of M and A cations, respectively.
* Single crystal used for structural study.
† Fragment from which the corresponding single crystal was selected.

Si = 3 (Table 6), although this method transfers all errors of the Si determination to the other cations in the formula, resulting in larger absolute errors on the number of cations (Ercit 2002). The $Me^{2+}/Me^{3+}$(Me = Mn, Fe) values were varied to balance the total sum of 25 negative charges. On the basis of their different redox potentials, all Fe was considered $Fe^{3+}$, while only a part of Mn was calculated as $Mn^{3+}$. Assuming vacancies, i.e., that no element would be missing or poorly determined in the analysis, even if all $Mn^{2+}$ is assigned to the octahedral sites, the amount of divalent octahedral cations ($Mn^{2+}$ + Mg) does not exceed 0.44 apfu. Even if all Mg is assigned to M3, this site appears to be dominated by trivalent cations. The excess of positive charge due to the REE incorporation would be mainly balanced by A-site vacancies (0.22–0.30 apfu). In other words, whenever the chemical data are normalized to Si = 3.00 apfu, the mineral from Kesebol would show an ideal formula $Ca(REE^{3+}_{2/3}\square_{1/3})Me^{3+}_3(SiO_4)(Si_2O_7)O(OH)$. However, as it will be shown below, it turned out that this hypothesis is wrong.

## Mössbauer data

The collected Mössbauer spectrum was fitted to three absorption doublets. Values of the isomer shifts (0.36 and 0.37 mm/s

for $Fe^{3+}$; 1.11 mm/s for $Fe^{2+}$) show that $Fe^{3+}$is present at least on two octahedral sites, one of which more distorted (quadrupole splitting = 1.96 mm/s) than the other one (quadrupole splitting = 1.02 mm/s). We note that the presence of $Fe^{2+}$(~12% of the total iron) in an octahedral site contradicts the interpretation of the chemical data reported above, where all Fe, and part of the Mn, were assumed as trivalent to balance the deficiency of positive charge due to A-site vacancies. On the contrary, the presence of $Fe^{2+}$ in the sample implies that manganese, due to its higher redox potential, should dominantly be present as $Mn^{2+}$ rather than as $Mn^{3+}$.

**Description of the structure**

The structure of the mineral from Kesebol shows the typical features of the monoclinic epidote specimens, in which $Si_2O_7$ and $SiO_4$ units are linked to two kinds of chains (parallel to the *b* axis) built by edge-sharing octahedra. One chain consists of M2 octahedra while the other chain is formed by M1 octahedra with M3 octahedra attached on alternate sides along its length. The smallest M2 octahedron has a strong preference for Al, whereas the occupancy of M1 and M3 depends on competing ions, with cations having larger ionic radii mainly ordered on the larger M3 octahedron. The overall structural arrangement gives rise to two types of cavities, a smaller one named A1, where Ca or $Mn^{2+}$ may be the dominant cation, and a larger one named A2, mainly occupied by REE with possible replacements of Ca, Pb, or Sr.

**Structural data of the untreated crystals**

The lattice parameters of the mineral from Kesebol (Table 2) are among the largest values observed for REE-rich epidote minerals (Gieré and Sorensen 2004; Hoshino et al. 2005; Tumiati et al. 2005; Lavina et al. 2006; Orlandi and Pasero 2006; Cenki-Tok et al. 2006). The unit-cell volume, ranging from 478.5(2) to 481.1(2) $Å^3$ for the untreated crystals, is less than that of ferriallanite [482.6(2) $Å^3$; Karthashov et al. 2002], where the M3 octahedron is fully occupied by divalent cations ($0.93Fe^{2+}$ + $0.07Mn^{2+}$) and M1 has $Fe^{3+}$ as dominant cation. As a general observation, the large unit-cell volume shown by REE-rich epidote minerals is mainly due to the expansion of the octahedral chains caused by the incorporation of divalent cations at M3 rather than to the REE incorporation in itself. The <A2-O> distance, in fact, is uninfluenced by the REE → Ca substitution (Bonazzi and Menchetti 1995). In all the untreated crystals (i.e., K1, K2, K4, K5) the mean <M3-O> distance (ranging between 2.169 and 2.180 Å) exceeds by far the value expected for the cation populations deriving from the chemical formulae reported in Table 6. The expected <M3-O> value can be calculated using the end-member <M3-O> distances derived from known interatomic distances for members of the epidote group. These distances were assumed as the following: $<Mn^{2+}\text{-}O>_{M3}$ = 2.197 Å from manganiandrosite-(Ce) (Cenki-Tok et al. 2006); $<Mn^{3+}\text{-}O>_{M3}$ = 2.063 Å from the regression line calculated on different natural and synthetic piemontites (Bonazzi and Menchetti 2004); $<Al\text{-}O>_{M3}$ = 1.968 Å, and $<Fe^{3+}\text{-}O>_{M3}$ = 2.055 Å using the data published by Bonazzi and Menchetti (1995); $<Mg\text{-}O>_{M3}$ = 2.124 Å was extrapolated assuming a cation population of 0.87 Mg + 0.13 $Fe^{3+}$ at M3 in dollaseite-(Ce) (Peacor and Dunn 1988). Using a simplified procedure for site assignment based on decreasing ionic radii to fill first the M3 site, the expected <M3-O> values calculated for K1 (2.116 Å) and K2 (2.087 Å) do not match the observed distances (2.180 and 2.169 Å, respectively). Analogously, using the chemical data of k4 and k5 grains as representative of the crystals K4 and K5 used for the structural study, the expected <M3-O> values (2.098 and 2.109 Å, respectively) are smaller than the observed distances (2.169 and 2.174 Å, respectively). The actual gap between observed and expected values could be even larger if we assume, realistically, part of the divalent cations (i.e., Mg) to be located on the M1 site. This feature seems to indicate that the calculation of the $Me^{2+}/Me^{3+}$ ratio was biased by the assumption of vacancies in the A sites. Furthermore, the sum of the electrons at A1 and A2 sites obtained from the refinement (ranging from ca. 71 to ca. 74 in the crystals studied) is significantly greater than the one expected from chemical analyses normalized assuming A-sites vacancies (ranging from ca. 62 to ca. 69).

For the reasons discussed above, in spite of the evidence from chemical data, we suspected the M3 site-population to be dominated by divalent cations. In particular, as the Mössbauer spectroscopy indicated that only a fraction (ca. 12%) of the total iron is present as $Fe^{2+}$ and taking into account the higher oxygen fugacity required to oxidize $Mn^{2+}$ to $Mn^{3+}$, a cation population ($Me^{2+}$, $Me^{3+}$), with $Mn^{2+} > Fe^{2+}$, was hypothesized for the M3 site. The number of electrons at the M1 site, ranging from 21.5 to 22.4 in the untreated crystals, indicates a dominance of $Fe^{3+}$ at this site. A comparison of the <M1-O> distances (Fig. 1a) with those of other epidote samples containing $Fe^{3+}$ on M1 supports this hypothesis, although the untreated crystals show values slightly higher than those predicted for a pure Al-$Fe^{3+}$ population. The M2 site shows a lesser $Fe^{3+}$ incorporation as inferred by the mean electron number, which ranges from 14.7 to 15.1 in the untreated crystals, and by the <M2-O> values (Fig. 1b). The high $Fe^{3+}$ contents on M1 and M2 sites is an unusual feature for epidote-group minerals, except for ferriallanite-(Ce) from Ulyn Khuren (type locality) where $^{M1}(Fe^{3+}) = 0.80$ and $^{M2}(Fe^{3+}) = 0.44$ apfu (Karthashov et al. 2002).

**Structural data of the crystal heated in air**

To verify the hypothesis that M3 is dominantly occupied by divalent cations, the structural changes induced by heat treatment in air (crystal K3) can be examined and compared with the results previously observed for allanite and REE-bearing piemontite (Bonazzi and Menchetti 1994). Upon heating these minerals in air, $Fe^{2+}$ and $Mn^{2+}$ oxidize and the charge balance is maintained by concomitant H loss. The following scheme may describe the reaction in terms of a coupled substitution: $^{M3}(Fe^{2+}, Mn^{2+}) + {}^{O10}(OH^-) \leftrightarrow {}^{M3}(Fe^{3+}, Mn^{3+}) + {}^{O10}(O^{2-})$. Oxidation of the divalent cations is made evident by a shortening of the mean <M3-O> distance, while the loss of H compensating the oxidation of $Fe^{2+}$ and $Mn^{2+}$ is mostly indicated by the variation of the donor-acceptor (O10-O4) distance. With regard to the unit-cell parameters, the contraction related to the ($Fe^{2+}$, $Mn^{2+}$) → ($Fe^{3+}$, $Mn^{3+}$) oxidation results in a decrease of the *ab*sinβ parameter (Fig. 2a), while the relaxing of the H bond, which is approximately directed along [001], weakens the link between the M2 and the M1 + M3 octahedral chains, resulting in a lengthening

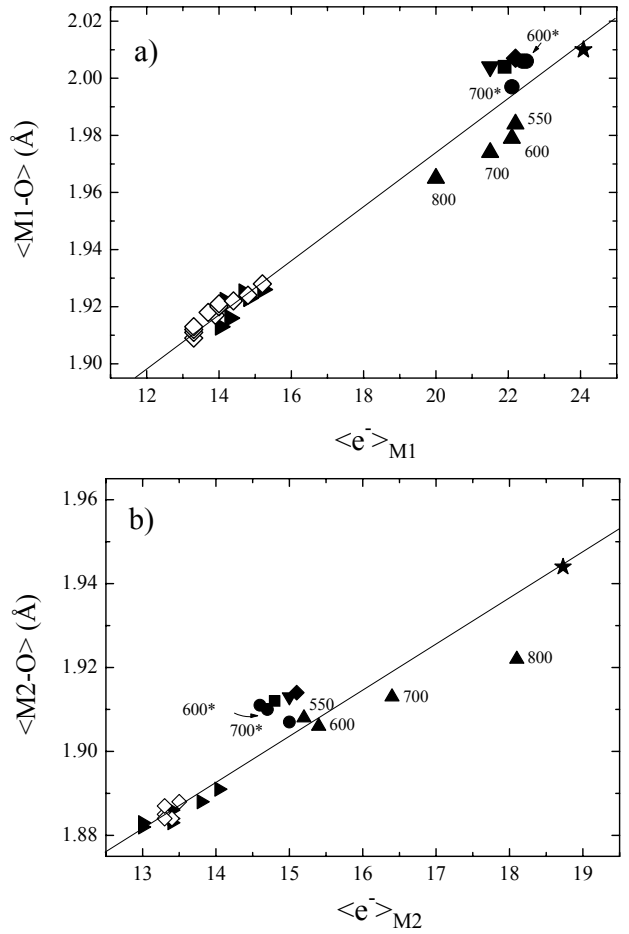


**FIGURE 1.** Mean <M1-O> distance vs. the electrons at the M1 site (**a**) and mean <M2-O> distance vs. the electrons at the M2 site (**b**). The equations of the regression lines [y = 1.786 + 0.0094× (*r* = 0.995) and y = 1.738 + 0.1105× (*r* = 0.994), respectively] were obtained using the literature data together with K5-700*. Symbols: filled diamond = K1; filled downward triangle = K2; filled upward triangles = K3; filled square = K4; filled circles = K5; filled rightward triangles = synthetic epidote specimens (Giuli et al. 1999); empty diamonds = natural epidote specimens (Bonazzi and Menchetti 1995); star = ferriallanite-(Ce) (Kartashov et al. 2002). Heating temperatures are indicated in °C; asterisks refer to thermal annealing under inert atmosphere.

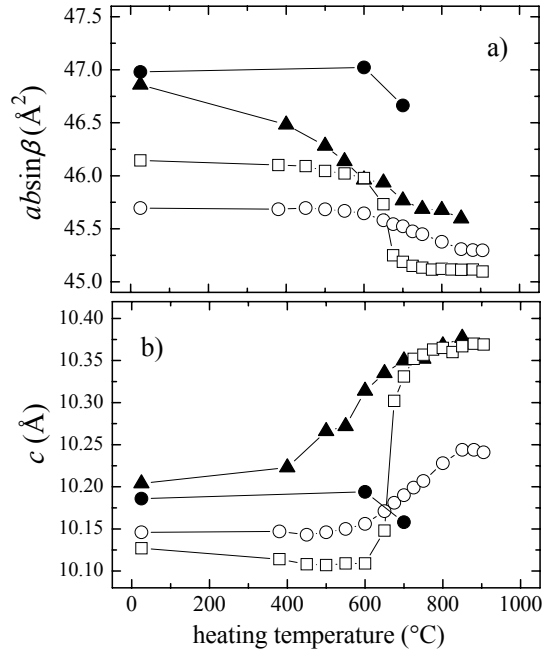


**FIGURE 2.** The *ab*sinβ product (**a**) and *c* parameter (**b**) plotted vs. the heating temperature. Symbols: filled upward triangles = K3 (heated in air); filled circles = K5 (heated under inert atmosphere); empty squares and empty circles refer to allanite (BG2 crystal) and REE-bearing piemontite (Br16a), respectively (Bonazzi and Menchetti 1994).

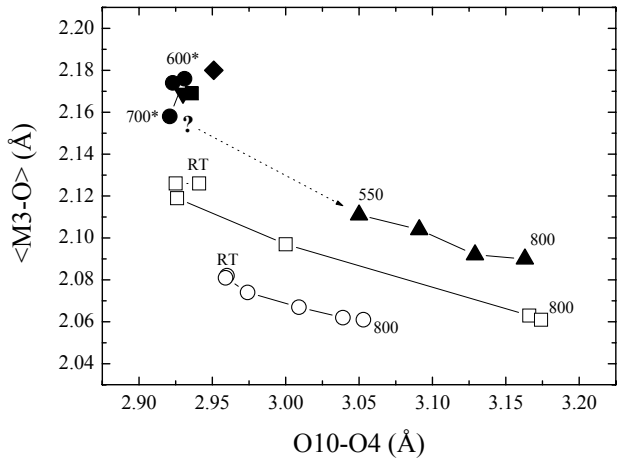


**FIGURE 3.** Reduction of the mean <M3-O> distance (indicating oxidation of divalent cations) and corresponding lengthening of the donor (O10)-acceptor (O4) distance (indicating H loss). Symbols: filled diamonds = K1; filled downward triangles = K2; filled upward triangles = K3; filled squares = K4; filled circles = K5; empty squares and empty circles refer to allanite (BG2 crystal) and REE-bearing piemontite (Br16a), respectively (Bonazzi and Menchetti 1994). Heating temperatures are indicated in °C; asterisks refer to thermal annealing under inert atmosphere.

of *c* (Fig. 2b). As shown in Figure 3, the behavior of <M3-O>, which decreases from 2.111 Å (K3-550) to 2.090 Å (K3-800) without any significant variation in the mean electron number at this site (Table 7) together with the corresponding increase of O10-O4 (up to 3.163 Å after heating at 800 °C) indicate oxidation of cations on M3 and corresponding dehydrogenation. Although the O10-O4 distance values observed in the untreated crystals (2.92–2.95 Å) are close to the value (2.941 Å) observed in the allanite BG2 (empty squares in Fig. 3) before heating, the value observed for K3-550 (3.050 Å) is noticeably higher than that observed for the allanite crystal at the same temperature (2.926 Å), thus suggesting that the dehydrogenation reaction develops at lower temperatures in this sample. By assuming the geometrical and structural parameters of the untreated K3 crystal be close to those of the other untreated crystals and, more properly, to those of the "restored" K5-700* crystal (see below), all the parameters indicating the ongoing of the oxidation-dehydrogenation process (i.e., <M3-O>, A2-O10, M2-O10 as the most sensitive) suggest a greater liability to oxidation with respect to the samples studied previously. Analogously, the values of the octahedral axes (Fig. 4) observed after the heating at 550 °C, are noticeably shorter

**TABLE 7.** Bond distances (Å), polyhedral volumes (Å$^3$), and selected parameters from the structure refinements

| | K1 | K4 | K2 | K5 | K5-600* | K5-700* | K3-550 | K3-600 | K3-700 | K3-800 |
|---|---|---|---|---|---|---|---|---|---|---|
| M1-O4 (×2) | 1.909(2) | 1.911(3) | 1.912(4) | 1.911(2) | 1.910(2) | 1.897(1) | 1.880(2) | 1.875(3) | 1.869(2) | 1.863(3) |
| M1-O5 (×2) | 2.058(2) | 2.052(3) | 2.053(4) | 2.056(2) | 2.057(2) | 2.047(1) | 2.046(3) | 2.047(4) | 2.042(2) | 2.037(4) |
| M1-O1 (×2) | 2.053(2) | 2.049(3) | 2.048(4) | 2.052(2) | 2.051(2) | 2.046(2) | 2.026(3) | 2.016(3) | 2.012(2) | 1.996(3) |
| mean | 2.007 | 2.004 | 2.004 | 2.006 | 2.006 | 1.997 | 1.984 | 1.979 | 1.974 | 1.965 |
| $V_{M1}$ | 10.73 | 10.68 | 10.68 | 10.73 | 10.72 | 10.56 | 10.34 | 10.27 | 10.19 | 10.04 |
| $\sigma^2$ | 5.86 | 6.55 | 6.61 | 5.81 | 6.06 | 6.81 | 10.18 | 10.50 | 12.14 | 13.03 |
| λ | 1.0040 | 1.0040 | 1.0040 | 1.0039 | 1.0040 | 1.0044 | 1.0057 | 1.0059 | 1.0064 | 1.0066 |
| s.s. | 22.2 | 21.9 | 21.5 | 22.4 | 22.5 | 22.1 | 22.2 | 22.1 | 21.5 | 20.0 |
| | | | | | | | | | | |
| M2-O3 (×2) | 1.889(2) | 1.888(3) | 1.894(4) | 1.885(2) | 1.886(2) | 1.884(1) | 1.892(3) | 1.891(3) | 1.912(2) | 1.927(4) |
| M2-O10 (×2) | 1.915(2) | 1.917(2) | 1.914(3) | 1.914(2) | 1.914(2) | 1.911(1) | 1.882(2) | 1.875(3) | 1.865(2) | 1.869(3) |
| M2-O6 (×2) | 1.938(2) | 1.932(2) | 1.931(3) | 1.932(2) | 1.934(2) | 1.926(1) | 1.949(2) | 1.953(3) | 1.961(2) | 1.970(3) |
| mean | 1.914 | 1.912 | 1.913 | 1.910 | 1.911 | 1.907 | 1.908 | 1.906 | 1.913 | 1.922 |
| $V_{M2}$ | 9.27 | 9.24 | 9.25 | 9.22 | 9.23 | 9.17 | 9.18 | 9.16 | 9.25 | 9.40 |
| $\sigma^2$ | 19.33 | 19.65 | 20.41 | 20.05 | 20.65 | 19.79 | 19.02 | 19.20 | 18.37 | 17.24 |
| λ | 1.0057 | 1.0057 | 1.0059 | 1.0059 | 1.0060 | 1.0058 | 1.0058 | 1.0060 | 1.0060 | 1.0058 |
| s.s. | 15.1 | 14.8 | 15.0 | 14.7 | 14.6 | 15.0 | 15.2 | 15.4 | 16.4 | 18.1 |
| | | | | | | | | | | |
| M3-O8 | 1.995(4) | 1.983(5) | 1.979(7) | 2.000(4) | 1.998(4) | 1.999(2) | 1.932(4) | 1.917(5) | 1.911(3) | 1.902(5) |
| M3-O4 | 2.061(4) | 2.052(4) | 2.051(5) | 2.057(3) | 2.062(3) | 2.035(2) | 1.965(4) | 1.957(4) | 1.931(3) | 1.911(4) |
| M3-O2 (×2) | 2.209(3) | 2.194(3) | 2.197(4) | 2.200(2) | 2.206(2) | 2.179(1) | 2.106(3) | 2.093(4) | 2.069(2) | 2.053(3) |
| M3-O1 (×2) | 2.303(3) | 2.295(3) | 2.294(4) | 2.292(3) | 2.293(2) | 2.277(1) | 2.278(3) | 2.281(4) | 2.287(2) | 2.309(4) |
| mean | 2.180 | 2.169 | 2.169 | 2.174 | 2.176 | 2.158 | 2.111 | 2.104 | 2.092 | 2.090 |
| $V_{M3}$ | 13.03 | 12.84 | 12.86 | 12.91 | 12.98 | 12.69 | 12.03 | 11.92 | 11.73 | 11.68 |
| $\sigma^2$ | 133.16 | 131.57 | 127.25 | 133.34 | 131.07 | 121.09 | 90.87 | 87.78 | 84.77 | 84.04 |
| λ | 1.0425 | 1.0422 | 1.0411 | 1.0422 | 1.0416 | 1.0387 | 1.0326 | 1.0324 | 1.0326 | 1.0342 |
| s.s. | 25.2 | 25.0 | 25.0 | 25.0 | 25.0 | 25.0 | 24.4 | 24.3 | 24.6 | 24.5 |
| | | | | | | | | | | |
| Si1-O7 | 1.598(4) | 1.596(4) | 1.588(6) | 1.596(4) | 1.598(3) | 1.590(2) | 1.584(4) | 1.590(5) | 1.584(3) | 1.576(5) |
| Si1-O1 (×2) | 1.642(3) | 1.647(3) | 1.645(4) | 1.644(2) | 1.645(2) | 1.640(1) | 1.646(3) | 1.648(3) | 1.641(2) | 1.638(3) |
| Si1-O9 | 1.640(4) | 1.642(4) | 1.641(6) | 1.643(4) | 1.635(3) | 1.637(2) | 1.636(4) | 1.630(5) | 1.629(3) | 1.618(5) |
| mean | 1.631 | 1.633 | 1.630 | 1.632 | 1.631 | 1.627 | 1.628 | 1.629 | 1.624 | 1.618 |
| $V_{Si1}$ | 2.217 | 2.225 | 2.212 | 2.221 | 2.217 | 2.200 | 2.207 | 2.211 | 2.188 | 2.164 |
| $\sigma^2$ | 9.19 | 8.79 | 9.93 | 9.54 | 9.19 | 10.10 | 9.38 | 9.15 | 9.55 | 8.71 |
| λ | 1.0026 | 1.0026 | 1.0030 | 1.0027 | 1.0027 | 1.0029 | 1.0030 | 1.0029 | 1.0030 | 1.0029 |
| | | | | | | | | | | |
| Si2-O8 | 1.601(4) | 1.604(4) | 1.595(6) | 1.602(4) | 1.590(4) | 1.593(2) | 1.609(4) | 1.609(5) | 1.606(3) | 1.596(5) |
| Si2-O3 (×2) | 1.628(3) | 1.632(3) | 1.627(4) | 1.632(2) | 1.632(2) | 1.628(1) | 1.622(3) | 1.620(3) | 1.619(2) | 1.614(3) |
| Si2-O9 | 1.650(4) | 1.642(4) | 1.639(6) | 1.638(4) | 1.646(3) | 1.637(2) | 1.631(4) | 1.636(6) | 1.633(3) | 1.639(5) |
| mean | 1.627 | 1.628 | 1.622 | 1.626 | 1.625 | 1.622 | 1.621 | 1.621 | 1.619 | 1.616 |
| $V_{Si2}$ | 2.207 | 2.210 | 2.186 | 2.203 | 2.199 | 2.186 | 2.184 | 2.186 | 2.177 | 2.163 |
| $\sigma^2$ | 2.25 | 2.71 | 3.31 | 2.82 | 3.07 | 2.93 | 2.46 | 2.12 | 2.37 | 2.67 |
| λ | 1.0007 | 1.0008 | 1.0009 | 1.0008 | 1.0010 | 1.0009 | 1.0006 | 1.0005 | 1.0006 | 1.0007 |
| | | | | | | | | | | |
| Si3-O2 (×2) | 1.638(3) | 1.640(3) | 1.636(4) | 1.636(2) | 1.638(2) | 1.632(1) | 1.641(3) | 1.642(3) | 1.647(2) | 1.648(3) |
| Si3-O6 | 1.651(4) | 1.652(4) | 1.650(5) | 1.648(3) | 1.647(3) | 1.647(2) | 1.638(3) | 1.637(5) | 1.636(3) | 1.646(4) |
| Si3-O5 | 1.667(4) | 1.671(4) | 1.667(5) | 1.663(3) | 1.664(3) | 1.656(2) | 1.660(4) | 1.665(5) | 1.668(3) | 1.664(5) |
| mean | 1.649 | 1.651 | 1.647 | 1.646 | 1.647 | 1.642 | 1.645 | 1.647 | 1.650 | 1.652 |
| $V_{Si3}$ | 2.273 | 2.286 | 2.271 | 2.261 | 2.266 | 2.246 | 2.266 | 2.274 | 2.286 | 2.296 |
| $\sigma^2$ | 30.39 | 27.66 | 26.59 | 30.14 | 29.83 | 29.59 | 22.63 | 19.73 | 18.18 | 16.81 |
| λ | 1.0076 | 1.0069 | 1.0066 | 1.0075 | 1.0074 | 1.0073 | 1.0056 | 1.0050 | 1.0046 | 1.0042 |
| | | | | | | | | | | |
| A1-O3 (×2) | 2.310(3) | 2.297(3) | 2.300(4) | 2.301(3) | 2.305(2) | 2.303(1) | 2.301(3) | 2.306(4) | 2.303(2) | 2.303(4) |
| A1-O7 | 2.344(4) | 2.335(4) | 2.330(6) | 2.332(4) | 2.335(3) | 2.325(2) | 2.314(4) | 2.312(5) | 2.320(3) | 2.335(5) |
| A1-O1 (×2) | 2.371(3) | 2.370(3) | 2.370(4) | 2.367(3) | 2.371(2) | 2.365(1) | 2.402(3) | 2.410(4) | 2.413(2) | 2.418(3) |
| A1-O5 | 2.581(4) | 2.581(4) | 2.574(5) | 2.573(3) | 2.579(3) | 2.561(2) | 2.531(4) | 2.520(5) | 2.504(3) | 2.506(4) |
| A1-O6 | 2.996(4) | 3.004(4) | 2.997(5) | 2.992(3) | 2.988(3) | 2.979(2) | 2.987(4) | 2.991(5) | 3.004(3) | 3.006(5) |
| mean | 2.469 | 2.465 | 2.463 | 2.462 | 2.465 | 2.457 | 2.463 | 2.465 | 2.466 | 2.470 |
| $^{VI}$<A1-O> | 2.381 | 2.375 | 2.374 | 2.374 | 2.378 | 2.370 | 2.375 | 2.377 | 2.376 | 2.381 |
| $\delta_{7\text{-}6}$ | 0.415 | 0.423 | 0.423 | 0.419 | 0.409 | 0.418 | 0.456 | 0.471 | 0.500 | 0.500 |
| s.s. | 23.1 | 23.2 | 23.1 | 22.6 | 22.6 | 21.7 | 23.0 | 22.7 | 21.9 | 21.4 |
| | | | | | | | | | | |
| A2-O7 | 2.330(4) | 2.327(4) | 2.330(6) | 2.328(4) | 2.326(3) | 2.315(2) | 2.301(4) | 2.297(5) | 2.301(3) | 2.300(5) |
| A2-O2 (×2) | 2.521(3) | 2.522(3) | 2.523(4) | 2.518(2) | 2.517(2) | 2.511(1) | 2.543(3) | 2.554(4) | 2.570(2) | 2.591(4) |
| A2-O10 | 2.576(4) | 2.572(4) | 2.579(5) | 2.581(3) | 2.582(3) | 2.563(2) | 2.451(4) | 2.416(5) | 2.389(3) | 2.357(5) |
| A2-O2 (×2) | 2.647(3) | 2.645(3) | 2.650(4) | 2.643(2) | 2.640(2) | 2.642(2) | 2.718(3) | 2.730(4) | 2.742(2) | 2.744(4) |
| A2-O3 (×2) | 2.864(3) | 2.865(3) | 2.860(4) | 2.857(3) | 2.857(2) | 2.830(2) | 2.759(3) | 2.748(4) | 2.716(2) | 2.706(4) |
| A2-O8 (×2) | 3.003(3) | 3.004(3) | 3.009(2) | 2.998(4) | 3.005(4) | 2.992(2) | 3.014(3) | 3.021(4) | 3.027(2) | 3.038(5) |
| mean | 2.698 | 2.697 | 2.699 | 2.694 | 2.695 | 2.683 | 2.682 | 2.682 | 2.680 | 2.682 |
| s.s. | 49.4 | 48.3 | 48.0 | 49.6 | 49.9 | 51.9 | 48.8 | 49.0 | 50.9 | 51.7 |
| O10-O4 | 2.951 | 2.936 | 2.930 | 2.923 | 2.931 | 2.921 | 3.050 | 3.091 | 3.129 | 3.163 |

*Note*: $\sigma^2$ and λ as defined by Robinson et al. (1971); s.s. = site scattering; $^{VI}$<A1-O> = average of the six shortest A1-O distances; $\delta_{7\text{-}6}$ = difference between the seventh (A1-O6) and the sixth (A1-O5) distance.

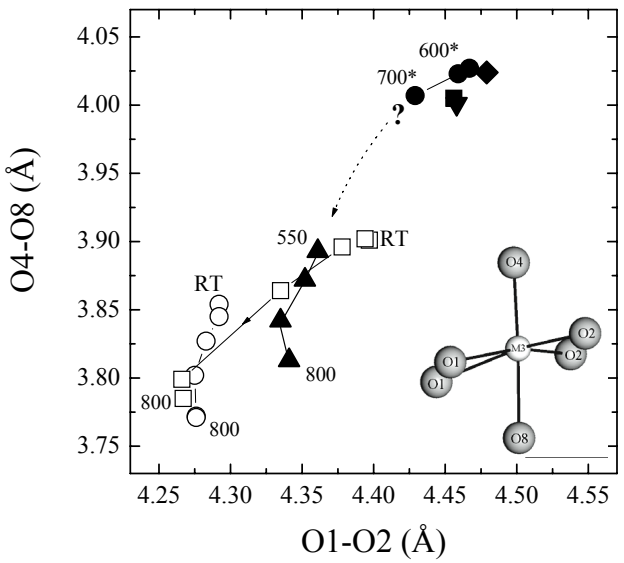


**FIGURE 4.** O4-O8 distance plotted vs. O1-O2; both are axial interatomic distances of the M3 octahedron. Symbols as in Figure 3.

than expected at this annealing temperature. However, the process is far from complete at 550 °C and the shrinking of the M3 octahedron goes on up to 800 °C following a path where the short axial O4-O8 distance decreases much more than the long axial O1-O2 distances. This feature, quite similar to that observed in the REE-bearing piemontite (empty circles in Fig. 4), is related to the oxidation of $Mn^{2+}$ leading to an increase of the Jahn-Teller active $d^4$ cation ($Mn^{3+}$), which has the electron hole in the $d_{Z^2}$ orbital along the O4-M3-O8 axis. On the contrary, in the case of allanite (empty squares in Fig. 4), the oxidation of $Fe^{2+}$ to $Fe^{3+}$ leads to an isotropic contraction of the M3 octahedron. Thus, we can suppose oxidation of $Fe^{2+}$ before 550 °C and of $Mn^{2+}$ in the 550–800 °C temperature range, respectively.

With the ongoing oxidation process, a moderate shortening of the <M1-O> distance occurs, mainly related to a decrease of the number of electrons on this site (Fig. 1a); on the contrary, as already observed for allanite and REE-bearing piemontite (Bonazzi and Menchetti 1994), the number of electrons on the M2 site increases (Fig. 1b) and the mean <M2-O> distance increases accordingly. An observation can be made about the migration of $Fe^{3+}$ from M1 to M2 with the increase of annealing temperature: the ability of M1 to house significant amounts of $Fe^{3+}$ is roughly related to the volume of the adjacent M3 octahedron sharing the O1-O4 edge. As the volume of the M3 octahedron progressively decreases in response to oxidation, M1 becomes prone to adjust the geometrical constraint by hosting increasing amounts of $Al^{3+}$ substituting for $Fe^{3+}$. The concomitant H loss allows the increase of $Fe^{3+}$ on M2: indeed, if H is present, M2 accommodates $Fe^{3+}$ with difficulty because of the very short M2-H distance (2.47 Å; Kvick et al. 1988).

The variation in the number of electrons on the A1 and A2 sites (Table 7), which occurs with the increase of the heating temperature, could be due to a migration of very minor amounts of REE from A1 to A2, thus suggesting that the high electron number found at A1 (ca. 23) for the untreated crystals does not correspond to a dominance of $Mn^{2+}$ in this site, but it is more likely due to a mixture of Ca, $REE^{3+}$, and $Mn^{2+}$. Indeed, the geometrical features ($^{VI}$<A1-O> and $\delta_{7\text{-}6}$ given in Table 7) of the A1 polyhedron do not support the dominance of $Mn^{2+}$ on this site (Bonazzi and Menchetti 2004; Cenki-Tok et al. 2006) in the sample from Kesebol.

### Structural data of the crystal heated under inert atmosphere ($N_2$)

It is well known (Mitchell 1973; Janeczek and Eby 1993) that mineral structures expand in response to metamictization, whereas restoring crystallinity results in a decrease of the unit-cell volume. Therefore, it was hypothesized that the exceptionally large unit-cell volume exhibited by the untreated crystals could be at least in part due to an expansion related to partial metamictization. The annealing under inert atmosphere at 700 °C, indeed, caused a rather isotropic contraction of the unit cell (i.e., *a*, *b*, and *c* shrank by 0.31, 0.33, and 0.27%, respectively; β unchanged). The variation of the unit-cell dimensions for the crystal annealed under inert atmosphere (K5) is well discernable from the variations caused by the oxidation and concomitant dehydrogenation induced by heating the crystal (K3) in air; in particular, the decrease of *c* observed for K5 testifies that no dehydrogenation occurred during annealing (Fig. 2b). Thus, the general, slight decrease of all the bond distances going from K5 to K5-700* is to be ascribed to a restoring of crystallinity rather than chemical modifications. The increase of crystallinity is also made evident by a considerable improvement of the quality of diffraction behavior (Table 2) and by the localization on the difference-Fourier map of a peak having atomic coordinates close to those commonly found for hydrogen in the allanite structure (Bonazzi and Menchetti 1995). On the contrary, for all the untreated crystals and for the crystals heated at $T < 700$ °C (under either inert or oxidizing atmosphere), a "ghost" peak approximately located at the barycenter of a tetrahedral cavity defined by O2-O2-O10-O4 atoms (Fig. 5) was observed. This peak has approximately the same coordinates of a peak (reported as hydrogen by Lavina et al. 2006) in the structure of the untreated, radiation-damaged dissakisite-(La). Thus, the

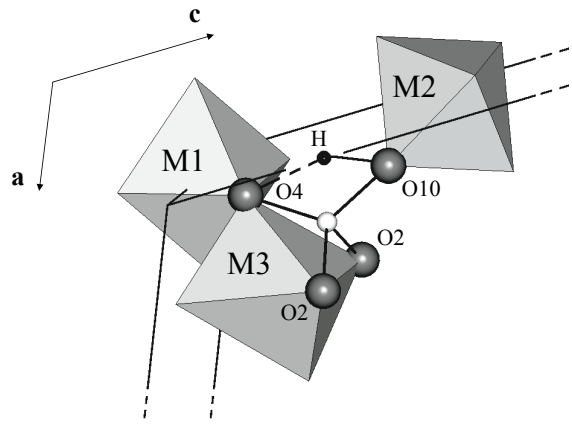


**FIGURE 5.** Tetrahedral cavity defined by the O2-O2-O10-O4 atoms with the "ghost" peak inside (white circle) observed for all the untreated crystals and for the crystals heated at $T < 700$ °C. In black, the H atom in the "regular" position as found in the crystal annealed under inert atmosphere (K5-700*).

presence of that "ghost" peak could be regarded as a sign of radiation damage.

No significant variation in the site scattering was observed except for the A1 and A2 sites where the electron number changes (–1.1 and +2.3 $e^-$, respectively), thereby confirming that heating induces re-ordering of REE on the A2 site. In contrast, no exchange of relevant amount of $Fe^{3+}$ between M1 and M2 occurs, thus corroborating the hypothesis that in K3 the migration of the octahedral cations is mainly driven by the oxidation-dehydrogenation reaction. As in the case of dissakisite-(La), the annealing produced a decrease of the displacement parameters [mean decrement of 37(4)%] leading to a significant increase in the number of the observed reflections. This feature, together with the slight contraction of the unit-cell parameters, supports the hypothesis that the structure of the mineral from Kesebol has expanded due to radiation damage. The observed shrinking due to recrystallization, however, was very small and the <M3-O> distance (2.158 Å) observed in the structure restored by annealing still indicates a dominance of divalent cations ($Mn^{2+}$, $Fe^{2+}$) at this site.

### Fourier-transform infrared microspectroscopy

The FTIR spectrum in the range 2000–4500 $cm^{-1}$ of an untreated sample is shown in Figure 6. The O-H stretching vibration results in a broad, asymmetrical band that appears to consist of two broad absorption peaks, around 3400 and 3250 $cm^{-1}$, respectively. As reported by Hoshino et al. (2005), there are two main O-H stretching peaks in unaltered and non-metamict allanite (at 3355 and 3187 $cm^{-1}$ for a sample from Daibosatsu Pass, Japan), which become broader and merge into a large band at lower wavenumbers with the increasing metamict state (3225, 3218, and 3209 $cm^{-1}$ for metamict allanite from Suishoyama, Fukudayama, and Shimo-ono, respectively). The position of the O-H stretching peaks in our sample, therefore, appears to be consistent with those expected for an essentially crystalline sample, in keeping with the X-ray diffraction quality. The wavenumbers, indeed, are even higher than those found by Hoshino et al. (2005) for non-metamict allanite. It should be taken into consideration, however, that the position of the main OH-stretching vibration in monoclinic epidote-group minerals strongly depends on composition (Liebscher 2004). The IR feature observed for the mineral from Kesebol is rather broad with respect to those reported for synthetic or natural epidote-group minerals (Langer and Raith 1974; Della Ventura et al. 1996; Langer et al. 2002). Besides the structural disorder associated with a slightly metamict state, the broadening observed could be related to the wide variety of configurations related to complex substitutions at the neighboring cation sites (M2, A2, M1, and M3) that lead to locally different values for A2-O10, M2-O10, M1-O4, and M3-O4 bond lengths.

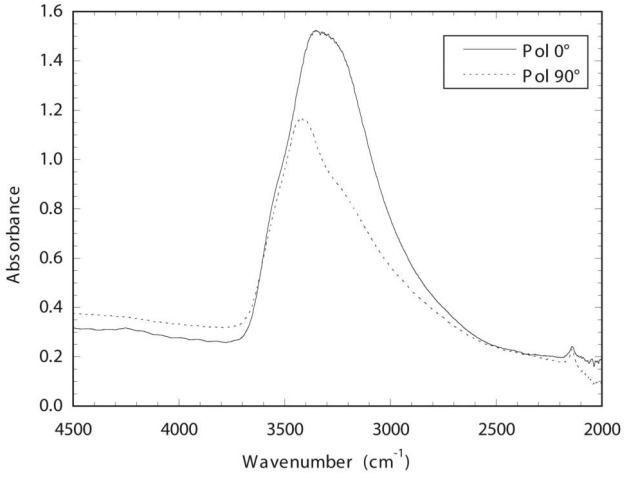


**FIGURE 6**. Infrared absorption spectra for the untreated mineral from Kesebol measured at two extinction positions found under crossed polars.

As it appears from Figure 6, there is a secondary peak at lower wavenumbers (~2140 $cm^{-1}$), which is never found in monoclinic epidote-group minerals, but closely resembles that observed in the infrared spectrum of zoisite at ~2170 $cm^{-1}$ (Liebscher 2004). Several interpretations were given for this feature in zoisite. On the basis of the pressure shift of this band, Winkler et al. (1989) hypothesized that it is related to an OH-bending vibration rather than to a stretching vibration and assigned the peak to the first overtone of the bending vibration of the O10-H···O4 hydrogen bridge. Nonetheless, as pointed out by Liebscher et al. (2002), the first overtone of the bending vibration of a straight hydrogen bridge should be in the range of ~1950–2000 $cm^{-1}$. These authors, therefore, interpreted the band at ~2170 $cm^{-1}$ as the first overtone of the bending vibration of the O10-H···O2 hydrogen bridge, whose bifurcated nature could explain the relatively high energy of this band. Although the hypothesis of a second proton position in zoisite needs to be proven by further studies focusing on polarized single-crystal IR spectroscopy (Liebscher et al. 2002), it seems worthy to note that the position of the "ghost" peak (Fig. 5) observed on the difference-Fourier map of all the untreated crystals roughly corresponds to the second proton position located between O10 and O2/O2′, as speculated by Liebscher et al. (2002) for the zoisite structure. Therefore, taking into consideration that the tetrahedral cavity defined by the O2-O2′-O10-O4 atoms is very similar either in the monoclinic or orthorhombic structure, we can hypothesize that in the untreated sample hydrogen, even locally, is disordered on two or more positions within the O2-O2-O10-O4 tetrahedral cavity.

### TEM-EDS results

A TEM-EDS investigation was carried out to find a reason for the apparent inconsistency between structural and chemical data. No evidence of crystalline phases other than "allanite" was found. Nonetheless, TEM bright field images revealed some microstructural heterogeneities at a submicrometer scale. In particular, areas affected by different degrees of radiation damage were found (Fig. 7, left column). The average microstructure of the sample appears with a mottled contrast typical of partially metamict samples, i.e., dark islands of crystalline material embedded in a bright, poorly crystalline matrix (Fig. 7a). Locally, metamict areas adjoining areas unaffected by radiation damage (Fig. 7b), as well as highly damaged areas embedded within relatively more crystalline areas (Fig. 7c) were observed.

High-resolution images actually confirmed the different degree of long-range order affecting these different microstruc-

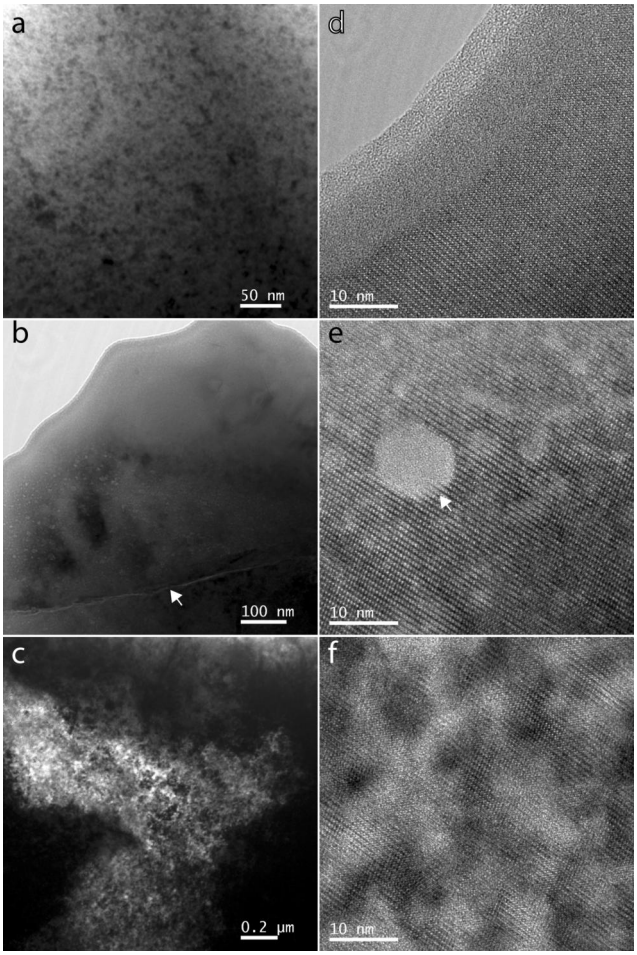


tures (Fig. 7, right column). Figures 7d and 7e were recorded in the upper right and lower left parts of Figure 7b, respectively. The former shows perfect long-range order, whereas the latter shows many damaged areas lacking of periodic structure, some of them with curious round shapes. It is not clear whether the latter are primary features, i.e., fluid inclusions, or radiation damage products. Finally, very low crystallinity (Fig. 7f) characterizes the bright areas of Figure 7c.

Selected area electron diffraction (SAED) patterns from the different microstructures also show relevant differences. For instance, Figure 8 refers to the [01$\bar{1}$] zone as obtained on the dark, crystalline area in Figure 7c (Fig. 8a) and on the central, bright, poorly crystalline area in Figure 7c (Fig. 8b). At a first glance, the intensity distribution among the transmitted beam, diffracted beams, and background is clearly different, with larger amount of diffuse scattering in Figure 8b. This difference is even more evident in the line-profiles taken along the *h*00 row given in Figures 8c and 8d, where the diffracted intensities are rescaled

◀**FIGURE 7**. TEM images of the mineral from Kesebol. Left column, bright field images: (**a**) mottled contrast typical of metamict minerals with crystalline dark areas (Bragg conditions); (**b**) a partially metamict area (lower left) adjoining an area unaffected by radiation damage (upper right). Note the fracture crossing the sample (arrow); (**c**) highly damaged area (bright) embedded in a relatively less damaged area (dark). Right column, high-resolution images of the [01$\bar{1}$] zone: (**d**) crystalline area from the upper-right part of the region imaged in b; (**e**) partially metamict area from the lower-left part of the region imaged in b. Note the round feature with amorphous contrast (arrow). Several similar features are visible at lower magnification in the damaged area imaged in b; (**f**) highly damaged area from the bright, central portion of the region imaged in c.

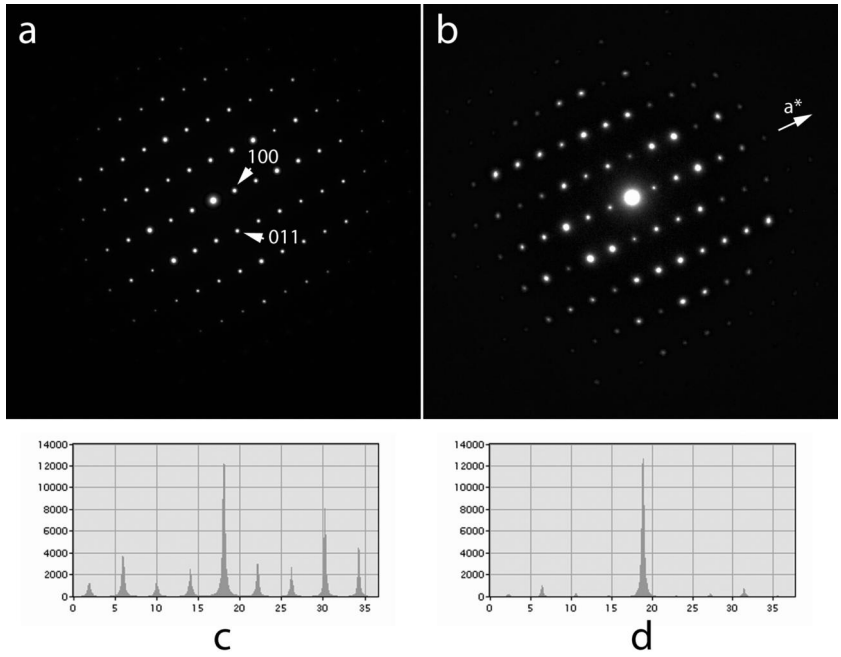


**FIGURE 8.** SAED patterns taken along the [01$\bar{1}$] zone representative of relatively crystalline (**a**) and highly damaged (**b**) regions reported in Figure 7c and relative line profiles (**c**, **d**) traced along the *h*00 row.

to that of the transmitted beam.

The different microstructures were checked for potential compositional differences by TEM-EDS analyses. We found that the more damaged areas are enriched in Si and O with respect to the more crystalline ones (Table 8; Fig. 9). In contrast, no relationship was found relating the REE content with the intensity of the damage. In keeping with Gieré and Sorensen (2004, and references therein), who reported that metamict samples tend to be more permeable to fluids than well-crystallized minerals, TEM results seem to indicated that $SiO_2$-rich fluid permeated the sample and altered preferentially the chemistry of the damaged areas. The fracture indicated by an arrow in Figure 7b might represent an imprint of the fluid passage toward the interior of the crystal.

## Discussion

The results of our TEM investigation suggest that chemical data are biased by the presence in the mineral of metamict areas enriched in $SiO_2$ and likely in $H_2O$, as inferred by low analytical totals (Table 1). EPMA data therefore need to be corrected for the excess of silica. With the assumption that (1) there are no significant vacancies in the A and M sites, and (2) fluids pervading the metamict areas led to a Si (and $H_2O$) enrichment only, chemical formulae were calculated on the basis of A + M = 5 and the excess of silicon (Si-3) was subtracted. $SiO_2$ (wt%) was modified accordingly and the chemical formulae were calculated on the basis of eight cations and 25 negative charges (Table 9). The method used to correct the analytical data are indeed rather rough; nonetheless, the cation population obtained with this procedure is in keeping with the structural and spectroscopic data. In particular, the cation populations on the A sites as given in Table 9 lead to a mean electron number [$\Sigma e^-$(A1 + A2) = 75.2 (K1), 74.4 (K2), 70.5 (k3), 71.0 (k4), and 73.8 (k5)] in satisfactory agreement with the site scattering obtained from the occupancy refinement for these sites [$\Sigma e^-$(A1 + A2) = 72.5 (K1), 71.1 (K2), 71.7–73.1 (K3), 71.2 (K4), and 72.2–73.6 (K5)]. Taking into account the high atomic number of the species ordered on A2 (REE and small amounts of Pb), the observed discrepancies (up to 3 electrons) may correspond to errors in the chemical formula of about 0.04–0.05 heavy atoms pfu. Thus, one can suppose that vacancies at the A2 site, if any, do not exceed 0.05 apfu. Even if small amounts of $REE^{3+}$ may also be accommodated at the A1 site, the A2 is still dominantly occupied by $REE^{3+}$, with $Ce^{3+}$ largely prevailing relative to the other lanthanides. The cation populations on the octahedral sites lead to a mean electron number [$\Sigma e^-$(M1 + M2 + M3) = 62.5 (K1), 62.3 (K2), 62.4 (k3), 62.3 (k4), and 62.4 (k5)] matching closely the site scattering obtained from the occupancy refinement for these sites [$\Sigma e^-$(M1 + M2 + M3) = 62.5 (K1), 61.5 (K2), 61.8–62.6 (K3), 61.7 (K4), and 62.1 (K5)]. The $Fe^{2+}/Fe_{tot}$ ratio of the formulae obtained with this procedure (Table 9) ranges from 0.10 to 0.15, in excellent agreement with the value estimated by Mössbauer data (Table 10). The total amount of divalent cations ($Mn^{2+}$ in the range 0.61–0.68 and $Fe^{2+}$ in the range 0.12–0.18) explains the large volume of the M3 octahedron, which has to be filled following a sequence based on decreasing ionic radii (i.e., Mg and $Fe^{3+}$) or by $Fe^{3+}$ and Al, if Mg is assumed to order on M1. Minor amounts of $Fe^{3+}$ (0.12–0.16 apfu in the non-oxidized crystals) can be assigned to M2, which is dominated by Al. Whatever the cation partition scheme adopted to fill M3, the remaining $Fe^{3+}$ is still enough to dominate the M1 site. As regards the octahedral sites, therefore, the key features of this REE-epidote, namely dominant $Fe^{3+}$ on M1 and dominant $Mn^{2+}$ on M3, are robust. In light of this, the most intense Lorentzian quadrupole doublet for $Fe^{3+}$ in the Mössbauer spectrum (Fig. 10) should be interpreted as due to $Fe^{3+}$ at M1, while the less intense doublet for $Fe^{3+}$ as due to the same cation at the more regular M2 octahedron (Table 10).

This $Fe^{3+}$-$Fe^{2+}$ distribution closely resembles that proposed

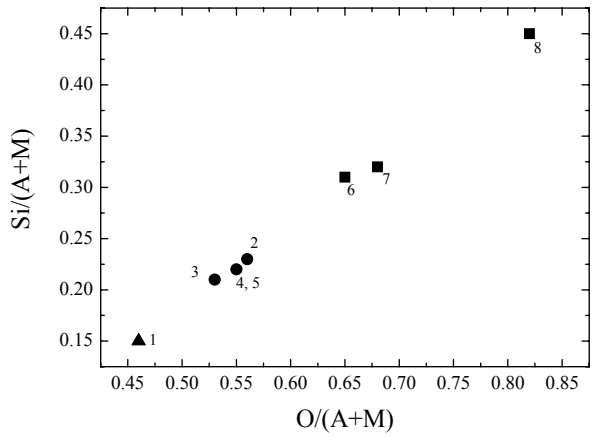


**Figure 9**. TEM-EDS microanalyses on different areas with different degree of metamictization: triangle = well-crystallized region; circles = slightly damaged areas; squares = strongly damaged areas. Labels refer to analytical data reported in Table 8. M includes Al, Fe, Mn, and Mg; A includes Ca, Ce, and Nd.

**Table 8.** TEM-EDS microanalyses on different areas differently damaged

| | 1 | | 2 | | 3 | | 4 | | 5(2) | | 6(2) | | 7 | | 8 | |
|---|---|---|---|---|---|---|---|---|---|---|---|---|---|---|---|---|
| | Element wt% | σ wt% | Element wt% | σ wt% | Element wt% | σ wt% | Element wt% | σ wt% | Element wt% | σ wt% | Element wt% | σ wt% | Element wt% | σ wt% | Element wt% | σ wt% |
| Mg | 0.08 | 0.22 | 0.26 | 0.21 | 0.36 | 0.19 | 0.55 | 0.28 | 0.36 | 0.09 | 0.45 | 0.13 | 0.31 | 0.21 | 0.95 | 0.29 |
| Al | 4.66 | 0.37 | 4.54 | 0.36 | 4.46 | 0.31 | 4.98 | 0.45 | 4.39 | 0.15 | 4.09 | 0.21 | 4.23 | 0.32 | 3.48 | 0.43 |
| Si | 11.63 | 0.53 | 14.25 | 0.57 | 14.18 | 0.48 | 14.20 | 0.68 | 13.67 | 0.24 | 17.01 | 0.38 | 17.73 | 0.59 | 21.39 | 0.89 |
| Ca | 5.02 | 0.34 | 5.83 | 0.35 | 6.00 | 0.30 | 5.92 | 0.42 | 6.27 | 0.16 | 5.10 | 0.21 | 5.33 | 0.32 | 4.86 | 0.41 |
| Mn | 9.86 | 0.63 | 10.99 | 0.65 | 9.83 | 0.51 | 10.75 | 0.77 | 10.52 | 0.28 | 8.57 | 0.37 | 9.70 | 0.60 | 5.90 | 0.69 |
| Fe | 17.19 | 0.77 | 13.01 | 0.69 | 13.27 | 0.57 | 13.16 | 0.80 | 13.88 | 0.30 | 13.00 | 0.42 | 11.87 | 0.63 | 9.49 | 0.78 |
| Ce | 15.51 | 1.09 | 14.96 | 1.11 | 14.73 | 0.89 | 13.87 | 1.27 | 15.62 | 0.48 | 15.50 | 0.67 | 14.53 | 1.02 | 13.59 | 1.32 |
| Nd | 5.23 | 1.28 | 3.40 | 1.26 | 4.35 | 1.01 | 3.36 | 1.46 | 2.98 | 0.56 | 1.87 | 0.78 | 1.18 | 1.19 | 3.17 | 1.43 |
| O | 30.82 | 1.10 | 32.76 | 1.08 | 32.82 | 0.92 | 33.21 | 1.31 | 32.34 | 0.45 | 34.44 | 0.66 | 35.12 | 1.01 | 37.19 | 1.39 |

*Notes*: (2) = average over two point analyses. 1 = highly crystalline area as in Figure 7d; 2 = partially damaged area as in Figure 7e; 3–5 = partially damaged areas as in Figure 7c (dark contrast); 6–8 = highly damaged areas as in Figure 7c (bright contrast).

**TABLE 9.** Final chemical formulae (after Si subtraction) for the epidote-group mineral from Kesebol

| | K1* | K2* | k3† | k4† | k5† |
|---|---|---|---|---|---|
| $SiO_2$‡ | 29.10 | 28.62 | 29.30 | 29.49 | 29.38 |
| Si | 3.00 | 3.00 | 3.00 | 3.00 | 3.00 |
| $Ti^{4+}$ | 0.04 | 0.04 | 0.05 | 0.06 | 0.05 |
| Al | 1.05 | 1.07 | 1.08 | 1.08 | 1.07 |
| $Fe^{3+}$ | 0.99 | 1.00 | 1.07 | 1.04 | 0.99 |
| Mg | 0.07 | 0.07 | 0.05 | 0.06 | 0.06 |
| $Mn^{2+}$ | 0.68 | 0.64 | 0.63 | 0.61 | 0.65 |
| $Fe^{2+}$ | 0.17 | 0.18 | 0.12 | 0.15 | 0.18 |
| ΣM | 3.00 | 3.00 | 3.00 | 3.00 | 3.00 |
| $\Sigma e^{-}$(M) | 62.5 | 62.3 | 62.4 | 62.3 | 62.4 |
| La | 0.04 | 0.03 | 0.03 | 0.03 | 0.04 |
| $Ce^{+3}$ | 0.59 | 0.55 | 0.51 | 0.52 | 0.56 |
| Pr | 0.04 | 0.06 | 0.04 | 0.03 | 0.04 |
| Nd | 0.18 | 0.18 | 0.15 | 0.16 | 0.16 |
| Sm | 0.03 | 0.02 | 0.02 | 0.02 | 0.03 |
| Gd | 0.00 | 0.01 | 0.00 | 0.00 | 0.01 |
| ΣREE | 0.88 | 0.85 | 0.75 | 0.76 | 0.84 |
| Ca | 0.97 | 0.96 | 1.04 | 1.02 | 1.00 |
| $Mn^{+2}$ | 0.14 | 0.18 | 0.20 | 0.21 | 0.15 |
| Pb | 0.01 | 0.01 | 0.01 | 0.01 | 0.01 |
| ΣA | 2.00 | 2.00 | 2.00 | 2.00 | 2.00 |
| $\Sigma e^{-}$n.(A) | 75.2 | 74.4 | 70.5 | 71.0 | 73.8 |

*Notes*: Atomic ratios calculated from the analytical data given in Table 1 on the basis Σ(A + M) = 5.00 apfu and forcing Si = 3.00; FeO-$Fe_2O_3$ partitioned to balance 25 negative charges; $\Sigma e^{-}$(M) and $\Sigma e^{-}$(A) refer to sum of electron number of M and A cations, respectively.
* Single crystal used for structural study.
† Fragment from which the corresponding single-crystal was selected.
‡ Value (in wt% of oxide) corrected for Si excess (see text).

**TABLE 10.** Mössbauer parameters for the epidote-group mineral from Kesebol

| | IS* (mm/s) | QS† (mm/s) | Abs. area (%) |
|---|---|---|---|
| $^{M1}Fe^{3+}$ | 0.37(1) | 1.96(2) | 56(4) |
| $^{M2}Fe^{3+}$ | 0.36(1) | 1.02(2) | 32(3) |
| $^{M3}Fe^{2+}$ | 1.11(1) | 1.90(2) | 12(2) |

*Note*: Peak widths were constrained to the same value and iterated to 0.51(2); $\chi^2 \sim 3$.
* Isomer shift.
† Quadrupole split.

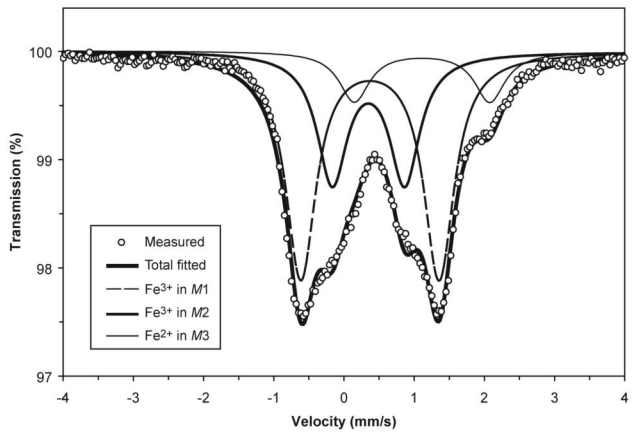


**FIGURE 10.** Observed and fitted Mössbauer spectrum for the untreated mineral from Kesebol.

for ferriallanite-(Ce) from the type locality (Kartashov et al. 2002) and of ferriallanite-(Ce) from the Bastnäs deposit, Sweden (Holtstam et al. 2003). In both these cases and in the mineral from Kesebol the concurrent high occurrence of large divalent cations at M3 [$Fe^{2+}$ in ferriallanite-(Ce), $Mn^{2+}$ with minor amounts of $Fe^{2+}$ in the mineral from Kesebol] precludes M3 from hosting significant amounts of $Fe^{3+}$, which partitions between M1 and M2 rather than between M3 and M1 as commonly happens in the epidote-group minerals. The quadrupole splitting (QS = 1.90 mm/s) for $Fe^{2+}$ located at the strongly distorted M3 octahedron is similar to the quadrupole splitting (QS = 1.96 mm/s) for $Fe^{3+}$ at M1. This feature is different from that commonly observed for allanite [QS of $Fe^{2+}_{M3}$ in the range 1.63–1.83 and QS of $Fe^{3+}_{M1}$ in the range 1.01–1.36; Liebscher (2004)]. On the other hand, the QS values observed for the mineral from Kesebol match closely those observed in both ferriallanite-(Ce) from Ulyn Khuren and the Bastanäs deposit where the QS values for $Fe^{2+}$ at M3 (1.62 and 1.60 mm/s, respectively) are even smaller than those for $Fe^{3+}$ at M1 (1.78 and 1.82 mm/s, respectively).

## REMARKS ON NOMENCLATURE

Caution should be exercised in naming new species of partially or fully metamict minerals, where anion- and cation-exchange properties and high reactivity related to metamictization can induce chemical variations and progressive hydration. Moreover, increasing amorphization leads to optical and other physical isotropy as well as a decrease in mean refractive index and density, thus making the physical and optical properties rather meaningless although required in the description of a new mineral species. Nonetheless, some comments can be made regarding fitting the mineral from Kesebol into the current classification scheme of epidote-group minerals (Armbruster et al. 2006). Regardless of minor substitutions, the ideal chemical formula for the epidote-group mineral from Kesebol is $CaREEFe^{3+}AlMn^{2+}(Si_2O_7)(SiO_4)O(OH)$, which is related to ferriallanite-(Ce) by the substitutional vector $^{M3}(Mn^{2+}) \rightarrow {}^{M3}(Fe^{2+})$.

According to the recommended rules (Armbruster et al. 2006), to name an epidote-group mineral, priority should be given to the choice of subgroup, then root name, and last the specific name. Because there are no uncertainties about the dominant valence at M3, M1, and A2, i.e., 2+, 3+, and 3+, respectively, the mineral belongs to the allanite subgroup. The key cation-sites M3 and A1 (and, in principle, M2) determine the root name. No current approved root-name is appropriate for an end-member with M3 = $Mn^{2+}$ and A1 = Ca. Therefore, a new root name should be assigned to this mineral. Furthermore, when M1 is not occupied by dominant Al, the prefixes ferri, mangani, chromo, and vanado should be added to indicate dominant $Fe^{3+}$, $Mn^{3+}$, $Cr^{3+}$, and $V^{3+}$ on M1, respectively. Thus, the prefix "ferri" should be added to a possible new root-name for the mineral from Kesebol. Last, the dominant REE cation on A2 (i.e., Ce) should be added as an extended Levinson suffix (Levinson 1966; Bayliss and Levinson 1988).

## ACKNOWLEDGMENTS

Kjell Gatedal, Nordmarkshyttan, collected and donated the original specimen. The authors also thank M. Tiepolo for LA-ICP-MS analyses carried out at CNR-IGG, sezione di Pavia; heating experiments under inert atmosphere were possible with the help of D. Borrini (University of Florence) and A. Orlando (CNR-IGG, sezione di Firenze). H. Skogby, Swedish Museum of Natural History, helped with the FTIR spectra. The authors honor and remember the late Filippo Olmi (CNR-IGG, sezione di Firenze) for his invaluable contribution to EPMA analyses.

The paper benefited greatly from the official reviews made by M. Nagashima and A. Liebscher. L.B. and P.B. acknowledge the project "Cristallochimica di minerali a terre rare" (60% grant) supported by the University of Florence.

## REFERENCES CITED


Andréasson, P.G., Solyom, Z., and Johansson, I. (1987) Geotectonic significance of Mn-Fe-Ba and Pb-Zn-Cu-Ag mineralization along the Sveconorwegian-Grenvillian front in Scandinavia. Economic Geology, 82, 201–207.

Armbruster, T., Bonazzi, P., Akasaka, M., Bermanec, V., Chopin, C., Gieré, R., Heuss-Assbichler, S., Liebscher, A., Menchetti, S., Pan, Y., and Pasero, M. (2006) Recommended nomenclature of epidote-group minerals. European Journal of Mineralogy, 18, 551–567.

Bayliss, P. and Levinson, A.A. (1988) A system of nomenclature for rare-earth mineral species: Revision and extension. American Mineralogist, 73, 422–423.

Bonazzi, P. and Menchetti, S. (1994) Structural variations induced by heat-treatment in allanites and REE-bearing piemontite. American Mineralogist, 79, 1176–1184.

——— (1995) Monoclinic members of the epidote group: Effects of the Al ↔ $Fe^{3+}$ ↔ $Fe^{2+}$ substitution and of the entry of $REE^{3+}$. Mineralogy and Petrology, 53, 133–153.

——— (2004) Manganese in monoclinic members of the epidote group: Piemontite and related minerals. In A. Liebscher and G. Franz, Eds., Epidotes, 56, p. 495–552. Reviews in Mineralogy and Geochemistry, Mineralogical Society of America, Chantilly, Virginia.

Bonazzi, P., Menchetti, S., and Reinecke, T. (1996) Solid solution between piemontite and androsite-(La), a new mineral of the epidote group from Andros Island, Greece. American Mineralogist, 81, 735–742.

Cenki-Tok, B., Ragu, A., Armbruster, T., Chopin, C., and Medenbach, O. (2006) New Mn- and rare-earth-rich epidote-group minerals in metacherts: Manganiandrosite-(Ce) and vanadoandrosite-(Ce). European Journal of Mineralogy, 18, 569–582.

Chesner, C.A. and Ettlinger, A.D. (1989) Composition of volcanic allanite from the Toba Tuffs, Sumatra, Indonesia. American Mineralogist, 74, 750–758.

Deer, W.A., Howie, R.A., and Zussman, J. (1986) Rock-Forming Minerals. Vol. 1b: Disilicates and Ring Silicates, second edition. Longman, Harlow, U.K.

Della Ventura, G., Mottana A., Parodi, G.C., and Griffin, W.L. (1996) FTIR spectroscopy in the OH-stretching region of monoclinic epidotes from Praborna (St. Marcel, Aosta Valley, Italy). European Journal of Mineralogy, 8, 655–665.

Drake, M.J. and Weill, D.F. (1972) New rare earth elements standards for electron microprobe analysis. Chemical Geology, 10, 179–181.

Ercit, T.S. (2002) The mess that is allanite. Canadian Mineralogist, 40, 1411–1419.

Geijer, P. (1961) The manganese, iron and copper mineralization at Kesebol in Dalsland, southwestern Sweden. Bulletin of the Geological Institutions of the University of Uppsala, New Series, 40, 37–49.

Gieré, R. and Sorensen, S.S. (2004) Allanite and other REE-rich epidote-group minerals. In A. Liebscher and G. Franz, Eds., Epidotes, 56, p. 431–493. Reviews in Mineralogy and Geochemistry, Mineralogical Society of America, Chantilly, Virginia.

Giuli, G., Bonazzi, P., and Menchetti, S. (1999) Al-Fe disorder in synthetic epidotes: A single-crystal X-ray diffraction study. American Mineralogist, 84, 933–936.

Grew, E.S., Essene, E.J., Peacor, D.R., Su, S.C., and Asami, M. (1991) Dissakisite-(Ce), a new member of the epidote group and the Mg analogue of allanite-(Ce), from Antarctica. American Mineralogist, 76, 1990–1997.

Holtstam, D., Andersson, U.B., and Mansfeld, J. (2003) Ferriallanite-(Ce) from the Bastnäs deposit, Västmanland, Sweden. Canadian Mineralogist, 41, 1233–1240.

Hoshino, M., Kimata, M., Nishida, N., Kyono, A., Shimizu, M., and Takizawa, S. (2005) Crystal chemistry of allanite from the Daibosatsu Pass, Yamanashi, Japan. Mineralogical Magazine, 69, 403–423.

Hoshino, M., Kimata, M., Shimizu, M., Nishida, N., and Fujiwara, T. (2006) Allanite-(Ce) in granitic rocks from Japan: genetic implications of patterns of REE and Mn enrichment. Canadian Mineralogist, 44, 31–44.

Ibers, J.A., and Hamilton, W.C. (1974) International Tables for X-ray Crystallography, vol. IV, 366 p. Kynock, Dordrecht, The Netherlands.

Janeczek, J. and Eby, R.K. (1993) Annealing of radiation damage in allanite and gadolinite. Physics and Chemistry of Minerals, 19, 343–356.

Jernberg, P. and Sundqvist, T. (1983) A versatile Mössbauer analysis program. University of Uppsala, Institute of Physics Report, UUIP-1090.

Kartashov, P., Ferraris, G., Ivaldi, G., Sokolova, E., and McCammon, C.A. (2002) Ferriallanite-(Ce), $CaCeFe^{3+}AlFe^{2+}(SiO_4)(Si_2O_7)O(OH)$, a new member of the epidote group: Description, X-ray and Mössbauer study. Canadian Mineralogist, 40, 1641–1648.

Kolitsch, U., Holtstam, D., and Gatedal, K. (2004) Crystal chemistry of $REEXO_4$ compounds ($X$ = P, As, V). I. Paragenesis and crystal structure of phosphatian gasparite-(Ce) from the Kesebol Mn-Fe-Cu deposit, Västra Götaland, Sweden. European Journal of Mineralogy, 16, 111–116.

Kvick, K.A., Pluth, J.J., Richardson Jr., J.W, and Smith, J.V. (1988) The ferric iron distribution and hydrogen bonding in epidote: A neutron diffraction study at 15 K. Acta Crystallographica, 844, 351–355.

Langer, K. and Raith, M. (1974) Infrared spectra of Al-Fe(III)-epidotes and zoisites, $Ca_2(Al_{1-p}Fe^{3+}_p)Al_2O(OH)(Si_2O_7)(SiO_4)$. American Mineralogist, 59, 1249–1258.

Langer, K., Tillmanns, E., Kersten, M., Almen, H., and Arni, R.K. (2002) The crystal chemistry of $Mn^{3+}$ in the clino- and orthozoisite-structure types, $Ca_2M^{3+}_3(OH/O/SiO_4/Si_2O_7)$: A structural and spectroscopic study of some natural piemontites and "thulites" and their synthetic equivalents. Zeitschrift für Kristallographie, 217, 563–580.

Lavina, B., Carbonin, S., Russo, U., and Tumiati, S. (2006) The crystal structure of dissakisite-(La) and structural variations after annealing of radiation damage. American Mineralogist, 91, 104–110.

Levinson, A.A. (1966) A system of nomenclature for rare-earth minerals. American Mineralogist, 51, 152–158.

Liebscher, A. (2004) Spectroscopy of epidote minerals. In A. Liebscher and G. Franz, Eds., Epidotes, 56, p. 125–170. Reviews in Mineralogy and Geochemistry, Mineralogical Society of America, Chantilly, Virginia.

Liebscher, A., Gottschalk, M., and Franz G. (2002) The substitution $Fe^{3+}$-Al and the isosymmetric displacive phase transition in synthetic zoisite: A powder X-ray and infrared spectroscopy study. American Mineralogist, 87, 909–921.

Mitchell, R.S. (1973) Metamict minerals: A review. Mineralogical Record, 4, 177–223.

Miyawaki, R., Yokoyama, K., Matsubara, S., Tsutsumi, Y., and Goto, A. (2008) Uedaite-(Ce), a new member of the epidote group with Mn at the A site, from Shodoshima, Kagawa Prefecture, Japan. European Journal of Mineralogy, 20, 261–269.

Nysten, P. and Holtstam, D. (2005) Crystal chemical data on Mn-rich "allanite" from the Harstigen and Kesebol Mn deposits, West Central Sweden. CER200—Rare Earth Minerals. GFF Stockholm 127, 38 (Abstract).

North, A.C.T., Phillips, D.C., and Mathews, F.S. (1968) A semiempirical method of absorption correction. Acta Crystallographica, A24, 351–359.

Orlandi, P. and Pasero, M. (2006) Allanite-(La) from Buca della Vena mine, Apuan Alps, Italy, an epidote-group mineral. Canadian Mineralogist, 44, 63–68.

Peacor, D.R. and Dunn, P.J. (1988) Dollaseite-(Ce) (magnesium orthite redefined): Structure refinement and implications for F + $M^{2+}$ substitutions in epidote-group minerals. American Mineralogist, 73, 838–842.

Peterson, R.C. and MacFarlane, D.B. (1993) The rare-earth-element chemistry of allanite from the Grenville Province. Canadian Mineralogist, 31, 159–166.

Pouchou, J.-L. and Pichoir, F. (1991) Quantitative analysis of homogeneous or stratified microvolumes applying the model "PAP." In K.F.J. Heinrich and D.E. Newbury, Eds., Electron Probe Quantitation, p. 31–75. Plenum Press, New York.

Robinson, K., Gibbs, G.V., and Ribbe, P.H. (1971) Quadratic elongation: A quantitative measure of distortion in coordination polyhedra. Science, 172, 567–570.

Sokolova, E.V., Nadezhina, T.N., and Pautov, L.A. (1991) Crystal structure of a new natural silicate of manganese from the epidote group. Kristallografiya, 36, 330–333.

Sheldrick, G.M. (1997) SHELXL-97. A new structure refinement program. University of Göttingen, Germany.

Thomson, T. (1810) Experiments on allanite, a new mineral from Greenland. Transactions of the Royal Society of Edinburgh, 8, 371–386.

Tumiati, S., Godard, G., Martin, S., Nimis, P., Mair, V., and Boyer, B. (2005) Dissakisite-(La) from Ulter zone peridotite (Italian Eastern Alps): A new end-member of the epidote group. American Mineralogist, 90, 1177–1185.

van Achterbergh, E., Ryan, C.G., Jackson, S.E., and Griffin, W.L. (2001) Data reduction software for LA-ICP-Ms. In P.J. Sylvester, Ed., Laser Ablation ICPMS in the Earth Sciences: Principles and Applications. Mineralogical Association of Canada, Short Course Series, 29, 239–243.

Van Cappellen, E. and Doukhan, J.-C. (1994) Quantitative transmission X-ray microanalysis of ionic compounds. Ultramicroscopy, 53, 343–349.

Winkler, B., Langer, K., and Johannsen, P.G. (1989) The influence of pressure on the OH valence vibration of zoisite. Physics and Chemistry of Minerals, 16, 668–671.


MANUSCRIPT RECEIVED APRIL 15, 2008
MANUSCRIPT ACCEPTED AUGUST 1, 2008
MANUSCRIPT HANDLED BY DARBY DYAR